CHAPTER 21

STABLE VALENCE ANIONS OF NUCLEIC ACID BASES AND DNA STRAND BREAKS INDUCED BY LOW ENERGY ELECTRONS

JANUSZ RAK[1*], KAMIL MAZURKIEWICZ[1], MONIKA KOBYŁECKA[1], PIOTR STORONIAK[1], MACIEJ HARANCZYK[1], IWONA DĄBKOWSKA[1], RAFAŁ A. BACHORZ[2], MACIEJ GUTOWSKI[1,3], DUNJA RADISIC[4], SARAH T. STOKES[4], SOREN N. EUSTIS[4], DI WANG[4], XIANG LI[4], YEON JAE KO[4], AND KIT H. BOWEN[4]

[1]*Faculty of Chemistry, University of Gdańsk, Sobieskiego 18, 80-952 Gdańsk, Poland*
[2]*Lehrstuhl für Theoretische Chemie, Institut für Physikalische Chemie, Universität Karlsruhe (TH), D-76128 Karlsruhe, Germany*
[3]*Chemistry-School of Engineering and Physical Sciencs, Heriot-Watt University, Edinburgh EH14 4AS, UK*
[4]*Department of Chemistry, Johns Hopkins University, Baltimore, MD 21218, USA*

Abstract: The last decade has witnessed immense advances in our understanding of the effects of ionizing radiation on biological systems. As the genetic information carrier in biological systems, DNA is the most important species which is prone to damage by high energy photons. Ionizing radiations destroy DNA indirectly by forming low energy electrons (LEEs) as secondary products of the interaction between ionizing radiation and water. An understanding of the mechanism that leads to the formation of single and double strand breaks may be important in guiding the further development of anticancer radiation therapy. In this article we demonstrate the likely involvement of stable nucleobases anions in the formation of DNA strand breaks – a concept which the radiation research community has not focused on so far. In Section 21.1 we discuss the current status of studies related to the interaction between DNA and LEEs. The next section is devoted to the description of proton transfer induced by electron attachment to the complexes between nucleobases and various proton donors – a process leading to the strong stabilization of nucleobases anions. Then, we review our results concerning the anionic binary complexes of nucleobases with particular emphasize on the GC and AT systems. Next, the possible consequences of interactions between DNA and proteins in the context of electron attachment are briefly discussed. Further, we focus on existing proposal of single strand break formation in DNA. Ultimately, open questions as well perspectives of studies on electron induced DNA damage are discussed

Keywords: Nucleic Acid Bases, Low Energy Electron, Strand Break, Stable Anion, Proton Transfer

* Corresponding author, e-mail: janusz@raptor.chem.univ.gda.pl

M. K. Shukla, J. Leszczynski (eds.), Radiation Induced Molecular Phenomena in Nucleic Acids, 619–667.

21.1. DNA DAMAGE INDUCED BY LOW ENERGY ELECTRONS

The last decade has witnessed immense advances in our understanding of the effects of ionizing radiation on biological systems [1, 2]. DNA as a genetic information carrier is the most important species, among cellular components, prone to damage by high energy photons. The basic mechanism by which DNA damage was initially thought to occur was attributed to ionization via direct impact of high-energy quanta. In 1994 Nikjoo et al. [3] calculated the probabilities for the formation of photon-induced single- (SSBs) and double-strand breaks (DSBs) in DNA and suggested that the minimum photon energy needed to produce SSBs and DSBs is as much as 20 and 50 eV, respectively. However, later Prise et al. [4] invalidated the estimations of the Nikjoo's group through experimental studies where samples of dry plasmid DNA were irradiated with photons of energies in the 5–200 eV range. By using gel electrophoresis the quantum efficiency of both SSBs and DSBs were measured, demonstrating that damage occurs at photon energies as low as 7–8 eV (Figure 21-1). The discrepancy between the experimental and calculated threshold energies for strand break formation occurred due to the fact that the Nikjoo's model was based on the selected bond energies of DNA constituents, and that turned out to be an oversimplification.

Comparing the values of optical oscillator strengths for the dissociative electronic excited states of hydrocarbons with dipole oscillator strength distribution for DNA and liquid water, it was possible to estimate that ca. 20% of the energy deposited by high-energy particles in cellular material leads to the electronically excited species which may stabilize themselves via hetero- or homolytic dissociation, whereas the remaining energy induces ionization in the cellular material [1]. As a consequence, ionizing radiation interacts with DNA primarily via products of its interaction with cellular environment [5]. Since water is the most ubiquitous component in all

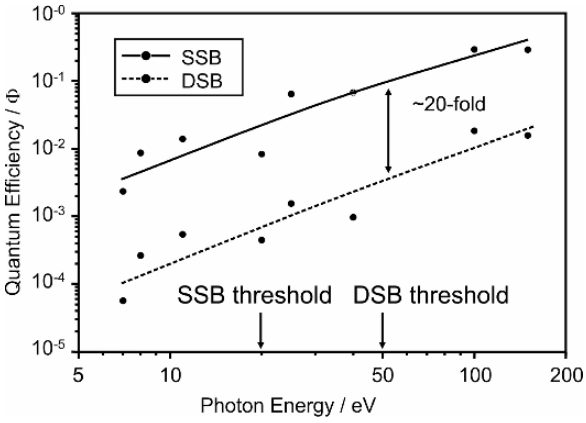

Figure 21-1. Quantum efficiency of SSB and DSB formation in dry plasmid DNA versus photon energy (Figure 3 of ref. [4]. Reprinted with permission.)

biological systems, most of the high energy radiation absorbed by living matter induces water radiolysis (generation of hydroxyl and hydrogen radicals) and the formation of secondary low-energy electrons (LEEs) [6]. LEEs are formed with the yield of ca. 4×10^4 per MeV of incident radiation [1, 7]. The secondary electron (SE) energy distribution has a maximum around 9–10 eV [8]. It was, however, unclear if such low-energy SEs are able to induce genotoxic damage (SSBs and DSBs) in DNA. To be specific, other secondary species, such as hydroxyl radicals, are known to be highly genotoxic [9, 10]. Indeed, abstraction of deoxyribose hydrogen atoms by $OH^{\bullet}$ radicals, formed through water homolysis by ionizing radiation, initiates at least one pathway which ends with the production of a DNA strand scission [9]. In Figure 21-2 the efficiency of DSB formation (in terms of the percent content of the linear forms of DNA determined with gel electrophoresis) induced by 8.5 eV photons in the water solution of DNA is displayed (N. Mason, private communication). Two variants of this experiment were performed – with and without radical ($OH^{\bullet}/H^{\bullet}$ atoms) scavengers – and their results allow one to draw the conclusion that low energy electrons themselves are able to generate DNA strand breaks.

Plasmid DNA was first bombarded with electrons of energies lower than 100 eV by Folkard et al. [11] who found threshold energies for SSB and DSB at 25 and 50 eV, respectively. Taking into account the fact that the majority of electrons formed within water radiolysis possess energies well below 30 eV, their finding suggested that LEEs are not necessarily an important factor in DNA damage. The paramount role of low energy electrons in the nascent stages of DNA radiolysis was only demonstrated by the pioneering works of Sanche and co-workers [1, 2]. In 2000 they published results of their seminal experiments concerning the irradiation of the thin layers of plasmid DNA with electrons of precisely determined energy [12–14]. Using gel electrophoresis to study irradiated samples they demonstrated

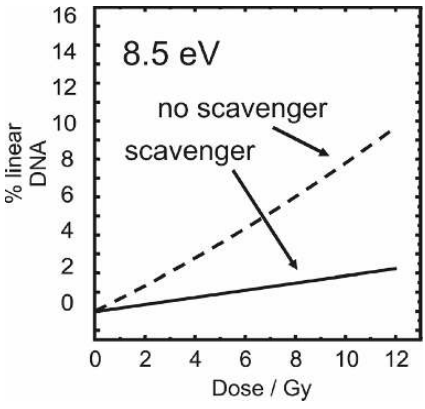

Figure 21-2. The effect of scavenger on the DSBs yields in DNA triggered by photons of 8.5 eV (N. Mason, private communication.)

unequivocally that electrons of sub-ionization energies (i.e. of energies lower than the ionization potential of DNA which are between 7.5 and 10 eV [13]) are capable of producing SSBs and DSBs in DNA (Figure 21-3). The incident electron energy dependence of damage to DNA was recorded between 3–100 eV in the single-electron regime [14]. The SSB yield threshold was registered near 4–5 eV (due to the cut-off of the electron beam at low energies [2]) whereas the DSB yield begins near 6 eV. Both yield functions possess a strongly structured pattern below 15 eV, have a peak around 10 eV, a pronounced minimum near 14–15 eV, a rapid increase between 15 and 30 eV, and above 30 eV roughly constant yields up to 100 eV.

Above 15 eV the mechanism of chemical bonds dissociation in DNA irradiated with LEEs is probably dominated by direct excitation of dissociative electronically excited states [15]. On the other hand, at lower energies the cleavage process is due to the formation of transient resonance anions [1, 2, 15–18]. Thus, the SSB and DSB maxima on the yield function observed around 8 and 10 eV (Figure 21-3),

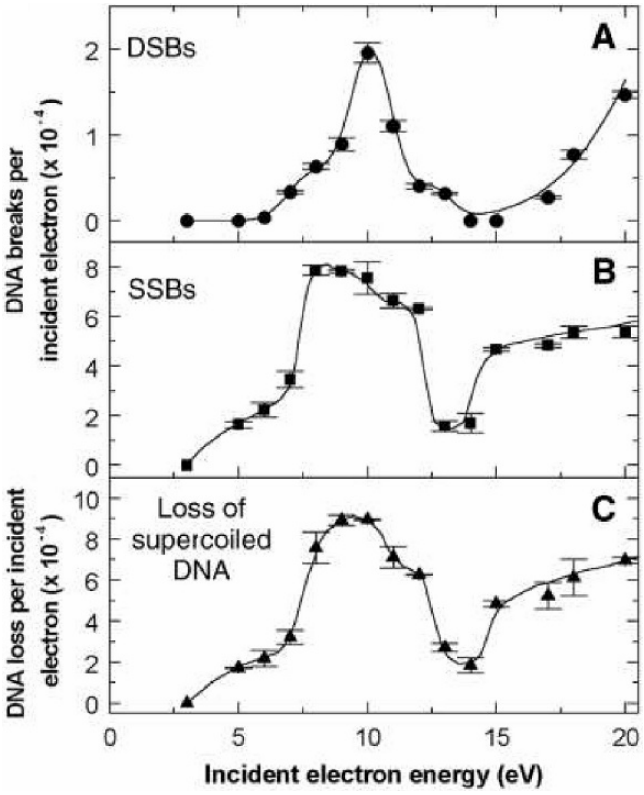

Figure 21-3. Measured quantum yields, per incident electron, for the induction of DSBs (A), SSBs (B), and loss of the supercoiled DNA form (C), in DNA solids by low-energy electron irradiation as a function of incident electron energy (Figure 1 of ref. [12]. Reprinted with permission from AAAS.)

respectively, may be interpreted as originating from resonance anions. The strand break yields as a function of electron impact energy peaks near the threshold for electronic excitation of DNA constituents which suggests that the cleavage process induced by electrons of 8–10 eV is initiated through the short-lived core-excited anion states [16]. The core-excited resonances usually have relatively long lifetimes which promote their dissociation [15]. Therefore, these species should play a key role in the direct dissociative electron attachment (DEA) process. Indeed, electron stimulated desorption (ESD) of anions from the LEE (3–20 eV) irradiated samples of plasmid and synthetic 40-base pair DNA duplex displayed maxima in the yield function of H^-, O^-, and OH^- around 9 eV [17]. The latter value falls in the 8–10 eV range where the main features in the yield functions of strand-break formation in DNA films are located (Figure 21-3). Thus, the ESD experiments together with the detection of SSBs and DSBs in damaged DNA samples suggest that core-excited resonances might decay in two ways: (i) via the direct DEA process that becomes a source of small molecular fragments desorbed into the gas phase, and (ii) through electron transfer to the phosphate group which in the next step(s) leads to the formation of SSB. Comparing the yield functions of H^- registered in the ESD experiments on DNA films [17] with that from ESD on films containing nucleobases [19], amorphous ice [20] and deoxyribose analogs [21] it was demonstrated that LEE-induced H^- desorption from DNA below 15 eV occurs mainly via DEA to nucleobases with some contribution from the deoxyribose ring [2]. Hence, in that energy range nucleobases seem to be primary targets for the interaction of LEEs with DNA.

At the lower energies of incident electrons (i.e. below 5 eV), shape resonances localized at nucleobases are suspected to be responsible for the observed strand damage [18, 22]. Due to the development of more sensitive techniques to assay SSB and DSB in DNA, the 0–4 eV range of incident electrons energies were studied by Martin and coworkers [18, 22] (Figure 21-4). This experimental picture could be reproduced by a model that simulates the electron capture cross-section as it might appear in DNA owing to the π^* anion states of the bases. The attachment energies were taken from the electron transmission measurements [23] and the peak magnitudes were scaled to reflect the inverse energy dependence of the electron capture cross-sections. The lowest peak in the modeled capture cross-section, which occurs at 0.39 eV in the gas phase, was shifted by 0.41 eV to match that in the SSB yield. The necessity of introducing this positive shift could be explained by the phosphate charge which in DNA is relatively close to the bases, thus producing a net destabilization which slightly exceeds that of the polarization induced by the transient anion [18]. The good agreement between the experimental and simulated SSBs yield functions in the 0–4 eV range may be considered as a strong argument confirming the involvement of shape resonances localized on nucleobases in the formation of LEE-induced strand breaks in DNA. An electron transfer mechanism involving shape resonances could also explain, at least partially, strand break formation by LEEs from the 8–10 eV range. First, for shape resonances the lifetime is usually too short above 5 eV for dissociation [16, 24] and electron

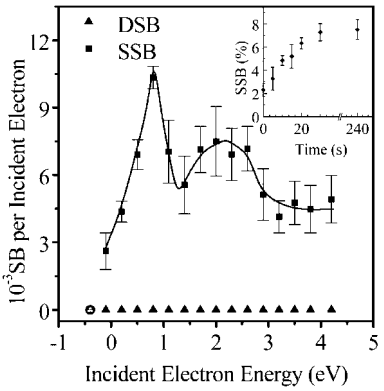

Figure 21-4. Quantum yield of DNA single strand breaks (SSBs) and double-strand breaks (DSBs) vs incident electron energy. The inset shows the dependence of the percentage of circular DNA (i.e., SSBs) on irradiation time for 0.6 eV electrons (Figure 1 of ref. [18]. Reprinted Figure with permission. Copyright 2004 by the American Physical Society.)

detachment or transfer is highly probable. Second, Grandi et al. [25] have reported the formation of a shape resonance for uracil near 9 eV. Consequently, this transient anionic state, which should also exist for nucleobases bound in DNA, could transfer its excess electron to unfilled orbitals of the phosphate group, lying close to 9 eV.

Recently, an electron transfer mechanism between transient anions (localized at nucleobases) and the phosphate group has been also suggested by experiments on short DNA fragments in which one of the bases was removed, leading to a DNA strand with an abasic site [26, 27]. For instance, the 10 eV resonance disappears at C-O bonds in the closest proximity to the abasic site (position 8 and 9; see Figure 21-5), whereas this resonance persists, causing damage at the other sites along the backbone.

Thus, in the single-strand GCAT tetramer, the formation of SSBs at the 8 and 9 sites (Figure 21-5) via transient anion formation is due to the presence of adenine. This observation can only be explained by invoking electron capture by adenine in GCAT followed by electron transfer to the backbone of DNA. Similarly, removal of adenine or guanine in the GCAT oligonucleotide leads to the reduction in the strand break damage for another resonance at 6 eV by a factor of ca. 6 [26]. The probability of strand breaks at different sites along the backbone of GCAT is strongly dependent on site and electron energy [6, 15, 26, 27], indicating that the nature and position of the base play a role in DNA damage, which seems to be an indirect evidence confirming that electron transfer from a base to phosphate is responsible for the SSBs formation. Furthermore, direct electron attachment to the phosphate groups should produce equal amounts of fragments for equivalent bonds. This is clearly far from being the case [6, 15, 26, 27] which implies that electron transfer from the bases to phosphate group is followed by the dissociation of the phosphodiester bond. Finally, electron transfer must account for the higher number

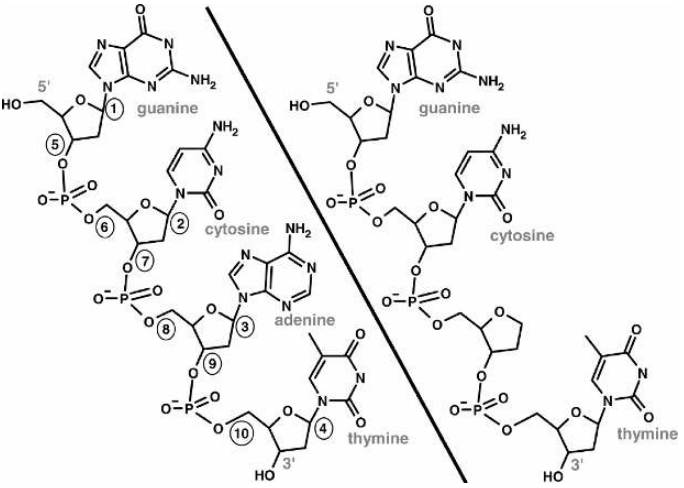

Figure 21-5. The molecular structure of tetramers GCAT and GCXT (X = stable abasic site) (Figure 1 of ref. [26]. Reprinted with permission. Copyright 2004 by the American Physical Society.)

of ruptured terminal phosphates observed for the GCAT tetramer irradiated with low energy electrons [6, 15, 26, 27].

Nearly all non-modified fragments of the tetramer irradiated by 4–15 eV electrons contained a terminal phosphate group, whereas fragments without this phosphate group, i.e., a terminal hydroxyl group, were negligible [15]. Thus, these results demonstrate that cleavage of the phosphodiester bond by 4–15 eV electrons takes place via the formation of a sugar radical and a phosphate anion, as also demonstrated in the analysis of the products obtained from DNA bombardment with 10 eV electrons [6]. By using an X-ray secondary electron emission source, Cai et al. [28] were able to directly compare DNA damage induced by high energy photons and LEEs under identical experimental conditions. They defined LEE enhancement factor (LEEEF) for monolayer (ML) DNA as the ratio of yield of products in ML DNA induced by the LEE ($E \leq 10$ eV) emitted from the metal substrate vs. the yield of products induced by the photons in a particular experiment. The extrapolated LEEEF for X-rays from 1.5 keV to 150 keV (i.e. to energies of medical diagnostic X-rays) is shown in Figure 21-6. It indicates that secondary electrons (SE) are 20–30 times more efficient at damaging DNA than the X-ray photons of 40–130 keV that create them which emphasizes the importance of interaction between SE and biological material for medical diagnostic and radiotherapy.

A picture that emerges from the above considerations can be summarized as follows. In contrast to the initial suppositions LEEs, the most abundant secondary product of interactions between condensed matter and ionizing radiation, turned out to be important damaging factor towards DNA. LEEs are ca. 30 times more efficient in the DNA cleavage than photons of the same energy. The resonance nature of damage seems to be well documented. Core-excited and shape resonances localized

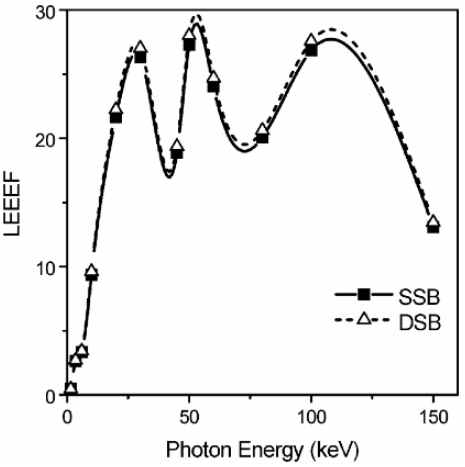

Figure 21-6. Low energy electron enhancement factor (LEEEF) as a function of photon energy for SSB and DSB production in a monolayer of DNA deposited on tantalum (Figure 14 of ref. [2]. Reprinted with permission. Copyright 2005 American Chemical Society.)

at nucleobases contribute significantly to the formation of DNA strand breaks. As a consequence the generation of the majority of strand breaks is preceded by electron transfer from the nucleobase anion to the phosphate group.

The currently accepted mechanism of single strand break formation involves through bond electron transfer (ET) which proceeds within non-adiabatic regime, i.e. directly from a resonant anion to the σ^* orbital of C3′-O or C5′-O bonds [2, 29]. This through bond electron transfer hypothesis is based exclusively on the computational results obtained by the Simon's group [29]. However, it is worth noting that there is no experimental evidence for that type of ET since products analysis was always carried out in the time frame several orders of magnitude longer (i.e. from microseconds to several hours) than that required for non-adiabatic ET to be completed. Furthermore, several studies concerning hole transfer in DNA, which do proceed in nonadiabatic manner [30] demonstrated that the rate of charge transfer is strongly modified by the conformational changes of the biopolymer [31, 32]. Hence, the dynamics of DNA might be another factor which could hinder the ET process assumed by the Simon's group [29] and the others [1, 2]. On the other hand, it is well known that the valence anions of nucleobases, unstable in the gas phase [33], become adiabatically stable due to even marginal solvation. For instance, employing photoelectron spectroscopy (PES) Bowen et al. [34] demonstrated that isolated uracil forms a stable dipole bound anion (DB). When it interacts with the argon atom both DB and valence anions are registered, and for uracil complex with single water molecule only the valence anion signal appears in the PES spectrum. Thus, the formation of stable anions in the DNA environment, where proton donors, polar and conjugated species are present seems to be quite probable. Indeed, an EPR signal that had to originate from the stable T^- and C^- anions was registered in the

past by Sevilla et al. [35]. As a consequence one can assume that the primary role of resonance states is to allow for energy transfer between the impinging electron and the neutral target [36]. In other words, we view anionic resonance states as doorways to bound valence anionic states. The latter may be involved in chemical transformations, such as DNA strand breaks, while the former are required to absorb excess electrons into the DNA environment [36]. If activation barriers associated with the cleavage of the stable anion were relatively low (less than 20–23 kcal/mol) the yield of SSBs function should have the shape reflecting the resonance cross-section since then electron attachment efficiency would directly affect the yield of strand breaks formation. This hypothesis is indeed consistent with the observed resonance structure in the damage quantum yield versus incident electron energy [12]. Moreover, the cleavage of *bound* anionic states does not have to compete with the very fast electron autodetachment process (ca. 10^{14} s^{-1}).

At the first glance it is not so obvious how within the 0–15 eV range the link between transient (metastable) and stable anions can be made. As we indicated above, the electron can be stabilized by proton transfer, however, one can wonder if this process is valid for the entire 0–15 eV range rather than only for near 0 eV electrons. It seems that there are four possible mechanisms that could link the initial transient anion to stable anions of the subunits of DNA: (i) vibrational stabilization triggered by the change in DNA configuration by the extra charge. The extra energy ($<$2 eV) of the electron is dispersed in vibrational excitation of DNA and then transferred to the surrounding medium. This mechanism, however, does not work for core-excited resonances; (ii) electron-emission decay of a core-excited shape resonance into an electronically excited state followed by vibrational stabilization; (iii) proton transfer stabilization, which neutralizes the anion charge while leaving a site with a ground state electron. This mechanism should work for any type of resonances; (iv) finally, superinelastic vibrational or electronic electron transfer [37]. This latter mechanism has been demonstrated for various molecules embedded in Kr solid and for N_2 in ice. In the last-mentioned case, the initial N_2^- ($^2\Pi_g$) state decays by electron emission into a trap within the H_2O matrix. In DNA, the initial anion would decay by electron emission to form a stable anion on another basic subunit.

The remaining part of this article demonstrates the possible involvement of stable nucleobases anions in the formation of DNA strand breaks – the concept which has been overlooked by the radiation research community so far. In Section 21.2 we describe proton transfer (PT) induced by electron attachment to the complexes between nucleobases and various proton donors – a process leading to the strong stabilization of nucleobases anions. We start with the description of methodology used to register the photoelectron spectra of anions. Next the basic characteristics of barrier free proton transfer (BFPT) induced by excess electrons in the complexes of nucleobases are described. Further, we review our results concerning the anionic binary complexes of nucleobases. Then excess electron induced BFPT/PT is characterized for the anions of AT and GC base pairs. Finally, the possible consequences of interactions between DNA and proteins in the context of electron attachment are

briefly discussed. In Section 21.3 we focus on existing proposal of single strand break formation in DNA. Ultimately, open questions as well perspectives of studies on electron induced DNA damage are discussed.

21.2. PROTON TRANSFER INDUCED BY ELECTRON ATTACHMENT IN THE COMPLEXES BETWEEN NUCLEOBASES AND PROTON DONORS

21.2.1. Experimental Methods: Anion Photoelectron Spectroscopy and Ion Sources

Negative ion photoelectron (photodetachment) spectroscopy is a powerful method for studying the electrophilic properties of molecules and complexes. During photodetachment, a photon ionizes the excess electron from a negative ion in a vertical process, almost instantaneously producing the anion's neutral counterpart in the geometry of the anion, viz., $X^- + h\nu \rightarrow X + e^-$, where the symbols, X^-, $h\nu$, X, and e^- respectively denote a negative ion, a photon of energy $h\nu$, the anion's neutral counterpart, and a free electron. Energetically, photodetachment is governed by the relationship, $h\nu = EBE + EKE$, where EBE is the electron binding energy (transition energy) in going from the ground state of the anion to a particular vibrational/electronic state of its corresponding neutral, and where EKE is the kinetic energy of the freed electron, corresponding to the residual energy of the photon after transition to a given vibronic state. Photodetachment is essentially the photoelectric effect applied to negative ions.

During photodetachment, the wavefunction of the anion (typically in $v'' = 0$) is reflected vertically (i.e., very quickly, without giving the nuclei of the system time to move) onto the wavefunctions of its corresponding neutral at the structure of the anion. The Franck-Condon overlap between these two sets of wavefunctions manifests itself as a spectral band in the photoelectron spectrum, viz., electron intensity vs. EBE (or EKE). The EBE of the intensity maximum in the lowest band observed is referred to as the vertical detachment energy, VDE. When there is overlap between the $v'' = 0$ wavefunction of the anion, X^-, and the $v' = 0$ wavefunction of its corresponding neutral, X, and when there is vibrationally resolved structure in the spectral band, an assignment of the spectrum locates the $v'' = 0 \rightarrow v' = 0$ (origin) transition and thereby provides the adiabatic (thermodynamic) electron affinity of X, i.e., EA_a (Figure 21-7). Such an assignment also yields the vibrational frequencies of the neutral. In addition, a Franck-Condon analysis can yield the structure of a simple anion, if the structure of its corresponding neutral is known. Furthermore, the width of the spectral band reflects the extent to which the structures of the anion and its neutral differ. A broad band implies a significant structural difference. Conversely, a very narrow band (peak width) implies nearly perfect Franck-Condon overlap, i.e., meaning that the structures of the anion and its neutral are essentially the same. This happens, for example, when weakly bound, dipole bound electron states are encountered. There are, of course, also additional

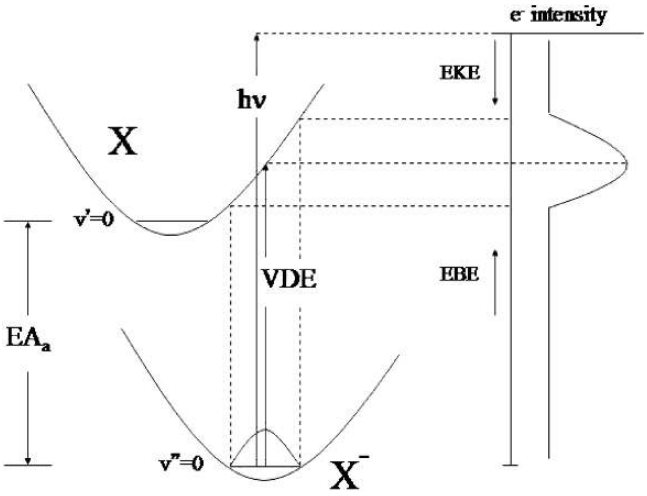

Figure 21-7. Energetic relationships between VDE, and EA_a

effects that may occur. For instance, when the anions being photodetached are vibrationally hot, v'' levels above $v'' = 0$ are also populated, and the electron intensity in the spectrum shows an onset at an EBE value below that of the $v'' = 0 \rightarrow v' = 0$ transition.

Anion photoelectron spectroscopy is conducted by crossing a mass-selected beam of negative ions with a fixed-frequency photon beam and energy-analyzing the resultant photodetached electrons (Figure 21-8). There are three main regions of such an apparatus; the source that generates the anions to be studied, the mass

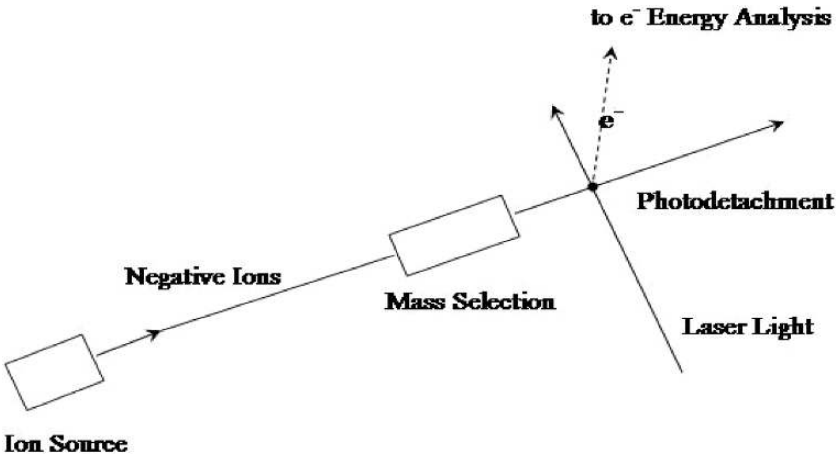

Figure 21-8. Schematic of a negative ion photoelectron (photodetachment) spectrometer

spectrometric selector/analyzer, and the photodetachment/electron energy analysis region. In order to maximize the types of systems that can be studied, we utilize two different types of anion photoelectron spectrometers. In one type (Figure 21-9a), anions are continuously generated by a source before being transported by ion optics through a magnetic sector which mass-selects them prior to photodetachment in the anion-photon interaction region. There, electrons are produced, and some of them are energy-analyzed by a hemispherical electron energy analyzer. In the other type of apparatus (Figure 21-9b), everything is done in a pulsed fashion. The anions are generated as ion pulses by the action of pulsed lasers, pulsed discharges, or pulsed gas valves. They then drift into the ion extraction region of a time-of-flight mass spectrometer, where they are accelerated to a common energy. Because they have different masses, they achieve different velocities, temporally separating their ion packets. Some distance away, they encounter a mass gate which allows only the selected masses to pass into the anion-photon interaction region. There, they are irradiated by a burst of photons from a pulsed laser. The resulting photodetached electrons are then energy-analyzed by passing through a magnetic bottle electron energy analyzer, which essentially performs a magnetically-guided, electron time-of-flight analysis of their kinetic energies. These two types of negative ion photoelectron spectrometers have their advantages and disadvantages, but they are also highly complementary. For example, continuous sources are well suited to gases and samples that can be thermally-evaporated, whereas pulsed sources can handle non-volatile substances and are especially well-situated for utilizing desorption processes. Sources are generally not inter-changeable between these two

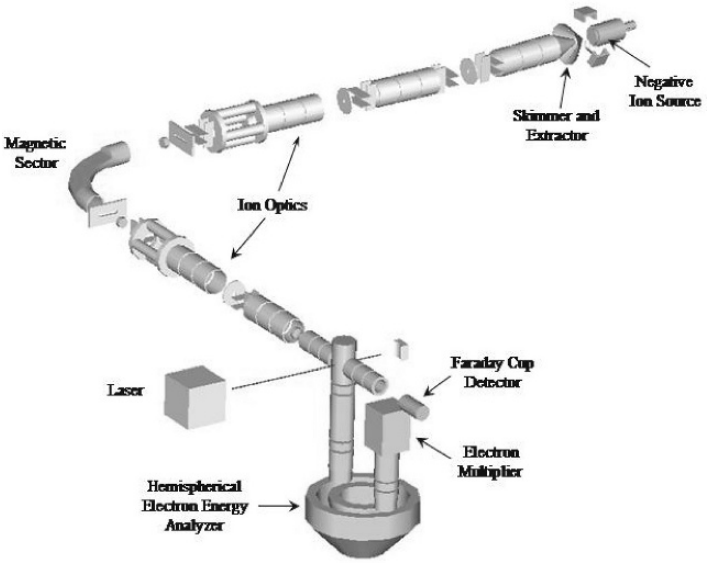

Figure 21-9a. Continuously-operating anion photoelectron apparatus

types of apparatus. Also, their mass-analyzer/mass-selectors are quite different. Our continuous machine uses a magnetic field to separate anions by their mass-to-charge ratios, and in the process, they are spatially dispersed. Our pulsed apparatus, on the other hand, uses time-of-flight mass analysis/mass selection, and in this case, the ions are temporally dispersed. The photon sources are also different. The continuous machine uses a continuously-running visible output, argon ion laser which is operated intra-cavity through the ion-photon interaction region in order to increase its already high photon power. The pulsed machine, however, utilizes a Nd:YAG laser in any of four harmonics. This gives the pulsed apparatus access to higher photon energies than are available on the continuous machine. Their electron energy analyzers are also quite different. The continuous apparatus utilizes a hemispherical deflector analyzer, while the pulsed machine uses a magnetic bottle. The hemispherical analyzer provides significantly higher resolution photoelectron spectra. Between the two types of apparatus, one can study almost any kind of system.

Anion sources are crucially important. Since the circumstances under which different anions can be formed vary widely, it is necessary to have access to a variety of sources. The nozzle-ion source (Figure 21-10) has been a workhouse for generating cluster anions. In this source, the substance from which anions are to be formed is placed in the stagnation chamber either as a solid, liquid, or gas, and argon gas is added to make-up the pressure to one or more atmospheres of pressure. Depending on the substance to be vaporized, the stagnation chamber may have to be heated or cooled to obtain the desired vapor pressure of sample. The resulting mixture of gases then expands (leaks) out of a tiny nozzle (~10–20 microns in diameter) into a high vacuum. The resulting adiabatic expansion can cool

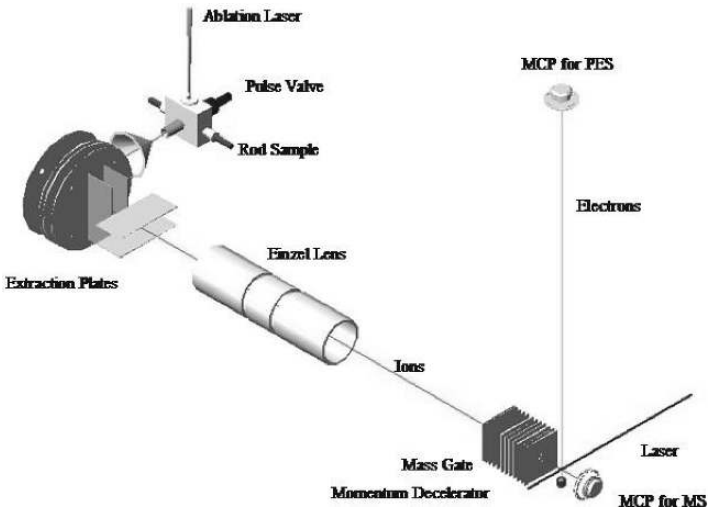

Figure 21-9b. Pulsed anion photoelectron apparatus

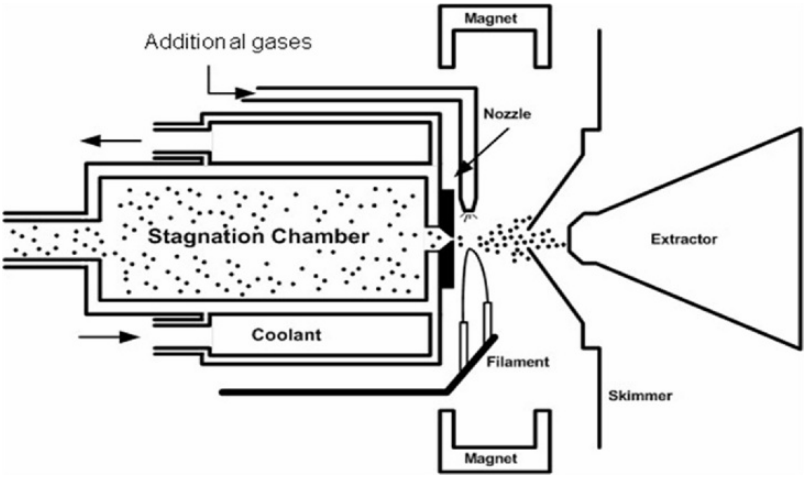

Figure 21-10. Schematic of a nozzle-ion source

the escaping gas mixture to very low temperatures (~20 K) causing clustering. Just outside the nozzle aperture is located a biased filament that pumps electrons directly into the expanding jet of gas. Nearby magnets provide a mostly axial magnetic field which helps to form a micro-plasma. The resulting mixture of gases and ions are then hydrodynamically skimmed before those ions having a negative charge are extracted into the ion optics of the apparatus. The stagnation chamber is biased (floated) at −500 volts, while the filament is biased ~50 volts more negatively to drive the electrons toward the nozzle. In some applications, additional gases are added to the plasma outside the nozzle.

Two sources that have been very useful in making cluster anions of involatile substances are the laser vaporization (Smalley) source and the pulsed arc discharge source (PACIS). Both of these sources inpart substantial energy to the samples they are vaporizing. In a laser vaporization source (Figure 21-11), a laser pulse strikes a rotating, translating rod of sample material (often a metal) producing a plasma. (Some versions of this source use rotating disks of sample material instead of rods.) Simultaneously, a burst of high pressure gas (typically helium) is admitted from behind the sample rod by a pulsed valve. The resulting "soup" of ions, neutrals, and helium, then expands out a nozzle into a high vacuum forming clusters and cluster ions.

The pulsed arc discharge source (Figure 21-12 [38]) also operates by pulsed vaporization of refractory materials. In this source, a pulsed discharge strikes a sample rod producing a plasma while a pulsed valve behind the discharge region admits a high pressure burst of helium gas. The resulting mixture of ions and neutrals then expands forming clusters and cluster anions. In some applications an extender (flow) tube is added to this source to allow the introduction of additional gases downstream.

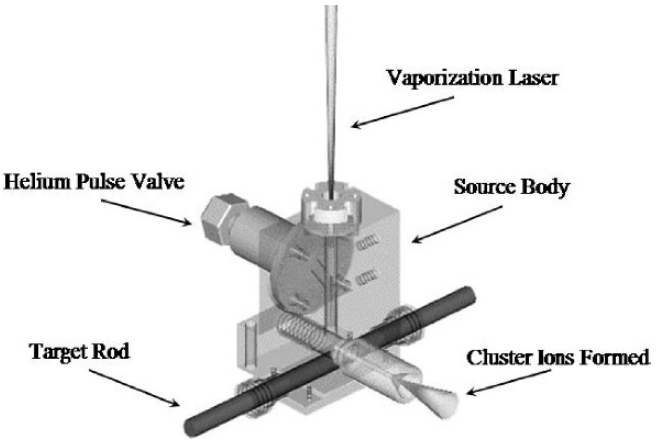

Figure 21-11. A laser vaporization ion source

When generating negative ions of biomolecules and their clusters, one faces a particular problem. While most biomolecules (beyond the smaller ones) are involatile, using high energy sources to vaporize the biomolecule sample very often simply destroys (cooks) it. Although these are well suited for generating rare tautomers of nucleic acid base anions, in most cases, gentler methods are required. If one wants to make parent anions, the situation is even more dire. Both electrospray and matrix isolated laser desorption ionization produce anions, but they are not usually parent anions. Typically, in negative ion mode, the biomolecules made with these sources have lost one or more hydrogen atoms, while in positive ion

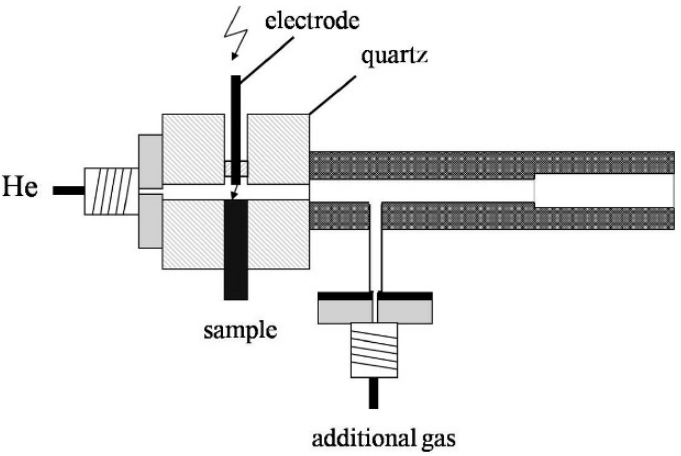

Figure 21-12. A pulsed arc discharge source (Figure 1 of ref. [38]. Reprinted with permission from AAAS.)

mode, they have been protonated. In addition, there is a tendency toward multiple-charging of the resultant ions. Basically, there were no sources that could reliably bring involatile biomolecules into the gas phase as intact parent anions. Since we often wanted to study the stable anions that result from the interaction of intact biomolecules with free electrons, we had to devise a new source. That source was the pulsed infrared desorption/pulsed photoelectron emission source (Figure 21-13). To design this source, we drew upon the work of Schlag [39] and of de Vries [40], who pioneered infrared desorption of biomolecules and upon the work of Boesl [41], who utilized pulsed lasers to make strong bursts of electrons. Our source functions as follows. A low intensity infrared laser pulse strikes a slowly moving bar of graphite which had been earlier prepared with a thin layer of the bimolecule of interest on its surface. Graphite absorbs infrared light well and the movement of the bar insures that each new laser pulse strikes a fresh surface of sample. The rapid heating of the 5–10 nsec. laser pulse causes the biomolecules to be flung into space, i.e., vaporized often without significant decomposition. After infrared desorption of the sample to produce a momentary puff of neutral biomolecules, a second laser (visible or ultraviolet) pulse strikes a nearby (~3 mm apart) rail of photoemitter (usually a metal wire) that is situated parallel to the graphite substrate bar. This pulse is much longer in intensity and produces a burst of electrons. The energy of these electrons can be adjusted by one's choice of the metal's work function. Then, almost simultaneously, a pulse of high pressure helium is admitted from behind the parallel bar and wire arrangement. Together, this results in a confluence of neutral intact biomolecules, low energy electrons, and a cooling jet of helium, and together they interact to form parent anions of biomolecules.

As an example of the capabilities of this source, we present the mass spectrum of the cytidine parent anion (Figure 21-14). This nucleoside anion would have been

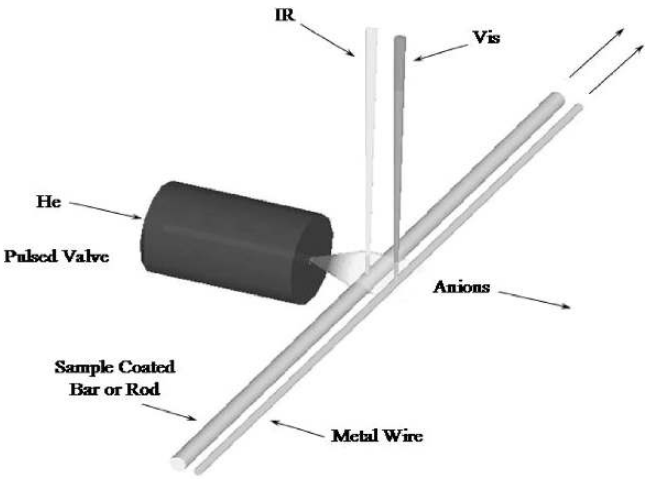

Figure 21-13. Schematic of a pulsed infrared desorption/pulsed photoelectron emission source

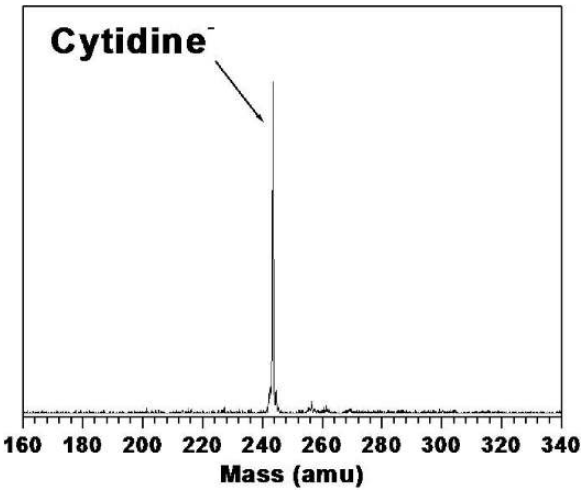

Figure 21-14. The mass spectrum of the cytidine parent anion which was brought into the gas phase by our pulsed infrared desorption/pulsed photoelectron emission anion source

extremely difficult (if not impossible) to get into the gas phase as an intact anion by conventional methods. We have also utilized this source to bring parent nucleotide anions and nucleotide/nucleoside dimer anions into the gas phase for study by anion photoelectron spectroscopy.

21.2.2. Basic Characteristics of Barrier Free Proton Transfer Induced by Electron Attachment

Described in the previous section, photoelectron spectroscopy has been employed by our experimental-theoretical group to study the electron affinity of binary complexes comprising nucleic acid bases [42–50]. The combination of this experimental technique with the computational methods of quantum chemistry turned out to be very successful and resulted in detailed description of barrier free proton transfer process (BFPT) induced by electron attachment to these complexes. For the first time this phenomenon was characterized in our work devoted to the anionic complex between uracil and glycine [42]. The basic features of BFPT were discussed in our highly correlated theoretical studies concerning the model anion of formic acid dimer $(FA)_2$ [51]. In order to describe the electron attachment process in this model system we calculated the electronic energies for the neutral and anionic complexes at the coupled-cluster level of theory with single, double, and perturbative triple excitations (CCSD(T)) [52] at the optimal second-order Møller–Plesset (MP2) geometries. These calculations were performed with augmented correlation-consistent basis sets of double- and triple-ζ quality, aug-cc-pVDZ and aug-cc-pVTZ, respectively [53]. The results of this work demonstrated that intermolecular proton transfer upon an excess electron attachment is not limited to complexes of nucleic

acid bases with weak acids [42–50] but is a common phenomenon in complexes bound by cyclic hydrogen bonds.

With PA and PD denoting proton acceptor and donor sites, respectively, we have computationally identified this process for the anionic dimers of formic acid (Figure 21-15a), formamide (Figure 21-15b), and in a heterodimer of formic acid with formamide (Figure 21-15c). The process has many similarities with that identified in anionic complexes of nucleic acid bases with weak acids [42–50]: (i) the unpaired electron occupies a π^* orbital, (ii) the molecular unit that accommodates an excess electron "buckles" to suppress the antibonding interactions the excess electron is exposed to, (iii) a proton is transferred to the unit where the excess electron is localized – thus the unpaired electron is stabilized, (iv) the minimum energy structure for the anion is characterized by two strong hydrogen bonds between the radical $[R\text{-}(PD)_2]^{\bullet}$ and the anion $[R'\text{-}(PA)_2]^-$, (v) the electron vertical detachment energy (VDE) is substantial ($1.6\,eV < VDE < 2.4\,eV$), whereas the monomers involved, such as formic acid or formamide, do not bind an excess electron in a valence anionic state.

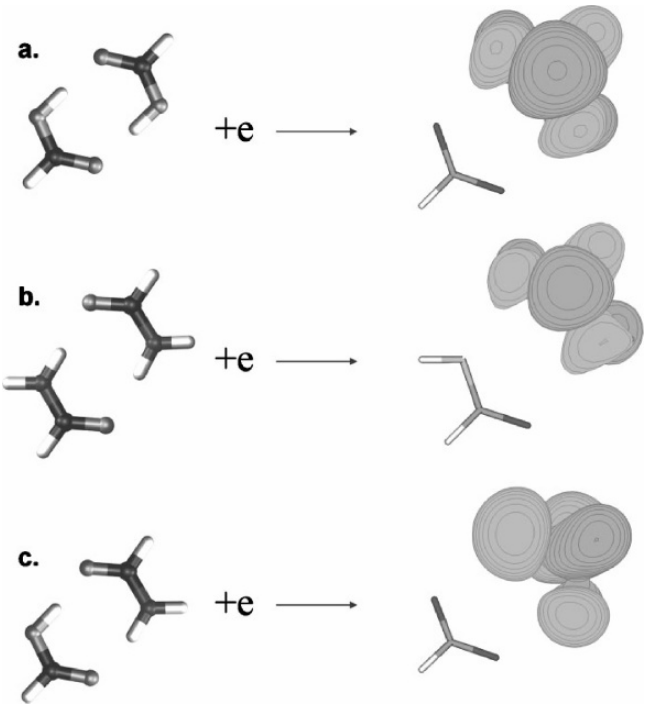

Figure 21-15. Attachment of an excess π^* electron to a cyclic hydrogen-bonded cluster facilitates intermolecular proton transfer: (a) formic acid dimer, (b) formamide dimer, and (c) formic acid-formamide (Figure 1 of ref. [51]. Reused with permission. Copyright 2005, American Institute of Physics)

The effects which proton transfer together with the buckling of monomer, that binds an excess electron, exert on the stability of the formic acid dimer anion are depicted in Figure 21-16. In Figure 21-16(a) the dihedral angle, *q* (H1-C1-O1-O2; Figure 21-16), describing the buckling of the formic acid monomer is decreased from 180° to 115° and the remaining geometrical degrees of freedom are optimized.

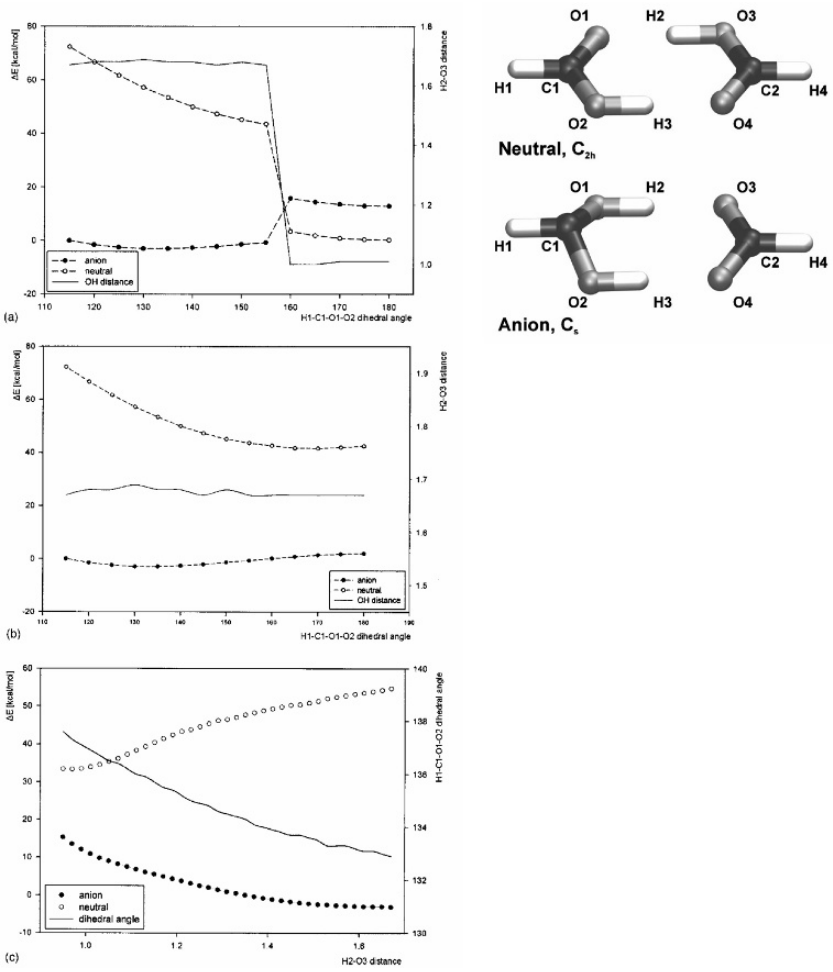

Figure 21-16. Plots of the relative electronic energy of neutral and anionic dimmers obtained at the B3LYP/TZVP+ level of theory in the course of partial geometry optimizations with fixed selected variables. The relative energies calculated with respect to the C_{2h} neutral. Bond lengths in Å, angles in deg. (a) The angle H1-C1-O1-O2 was *decreased* from 180° to 115° and the H2-O3 distance was displayed on the second vertical axis, (b) the angle H1-C1-O1-O2 was *increased* from 115° to 180° and the H2-O3 distance was displayed on the second vertical axis, (c) the H2-O3 distance was changed between 0.9 and 1.7 Å and the dihedral angle H1-C1-O1-O2 was displayed on the second vertical axis (Figures 2 and 3 of ref. [51]. Reused with permission. Copyright 2005, American Institute of Physics.)

The optimized H2-O3 distance does not exceed 1.05 Å for 160° < q < 180°, hence, the *R*′-(PA,PD)$^{\cdot\cdots}$(PD,PA)-*R* structure prevails. The anion remains unbound for this range of q. With the angle q further decreased, an intermolecular proton transfer occurs and the H2-O3 distance exceeds 1.45 Å for 115° < q < 155°. Thus the *R*′-$(PD)_2^{\cdot-}(PA)_2$-*R* structure prevails for this range of q. Moreover, the anionic state becomes vertically bound with respect to the neutral as a consequence of intermolecular proton transfer. In Figure 21-16(b) the case with the angle q being increased from 115° to 180° and the geometry optimization for the anion initialized in the neighborhood of the C*s* geometry of the anion is presented. The main finding is that the *R*′-$(PD)_2^{\cdot-}(PA)_2$-*R* structure is preserved even for q close to 180°. The *R*′-$(PD)_2$ unit remains nonplanar even for q equal to 180°, and the anion is vertically bound with respect to the neutral for the full range of q. Apparently, the intermolecular proton transfer is sufficient to stabilize the anion. In Figure 21-16(c) the case with the H2-O3 distance being changed between 0.95 and 1.67 Å is presented. Here, both the *R*′-(PA,PD)$^{\cdot\cdots}$(PD,PA)-*R* and the *R*′-$(PD)_2^{\cdot-}(PA)_2$-*R* structures are explored. The anion remains vertically bound with respect to the neutral even for the values of the H2-O3 distance as small as 1.0 Å and the values of q remain within a narrow range 132° < q < 138°. Apparently, the buckling of one of the monomers is sufficient to stabilize the anion.

Our computational results indicating the electron induced BFPT in $(FA)_2$ has been recently invoked to explain the dramatic difference between the monomer and the dimer of formic acid in the excitation of a vibrational quasicontinuum in the 1–2 eV range with the ejection of very slow electrons [54]. The value of deprotonation energy of a proton donor is one of the crucial factors deciding on the type of the complex anion(s) formed due to electron attachment. In the context of PT, the value of proton affinity of a proton acceptor is also an important characteristic. However, for most systems considered in this work the proton affinity of proton acceptor corresponds to that of a nucleobase anion. Thus for a series of complexes involving a given nucleobase, the occurrence of BFPT/PT is, in the first approximation, determined by the deprotonation energy of a proton donor. Basically, three types of systems, differing with the number and quality of anionic minima, are possible: (i) the anions that possess the same pattern of hydrogen bonds as their parent neutral counterpart (non-proton transfer (non-PT) structure), (ii) the anions for which both non-PT and PT structure are stable; these two minima are separated by, usually low, energy barrier for PT and (iii) the anions characterized by potential energy surface where only PT structure exists, i.e. systems where the attachment of electron triggers BFPT.

The relationships between the deprotonation energy of proton donor and complex stability as well as its VDE were characterized in our work devoted to complexes between uracil and a series of alcohols with deprotonation enthalpy (H_{DP}) varied in a systematic manner [48]. We found out that a H_{DP} smaller than 14.3 eV is required for BFPT with the product being UH$^{\bullet\cdots-}$OR. Two minima coexist on the anionic energy surface for 14.8 eV < H_{DP} < 14.3 eV. These minima correspond to the UH$^{\bullet\cdots-}$OR and U$^{-\cdots}$HOR structures. For ROH's with deprotonation enthalpies above 14.8 eV only the U$^{-\cdots}$HOR minimum exists on the potential energy surface.

In Figure 21-17 the dependence of the stabilization energy in anionic uracil-alcohol complexes vs. the deprotonation energy (E_{DP}) of alcohol (ROH) is shown [48]. On the other hand, Figure 21-18 depicts the variation in VDE with the E_{DP} of ROH [48].

The energy of stabilization of the anionic complex increases when acidity of alcohols increases (Figure 21-17). For anionic complexes for which we identified two minima corresponding to $U^{-\cdots}HOR$ and $UH^{\bullet\cdots -}OR$ structures, the structure with protonated uracil is more stable. The vertical detachment energy of anionic complex systematically increases when deprotonation energy of alcohol decreases. There is a discontinuity in VDE of ca. 0.5 eV, which is a manifestation of intermolecular proton transfer (Figure 21-18).

However, in order to predict the occurrence of proton transfer for a general case one cannot restrict themselves in their analysis to the deprotonation energy of proton donor (HA). The occurrence of intermolecular proton transfer results from a subtle interplay between the deprotonation energy of HA, protonation energy of nucleobase (NB), and the intermolecular stabilization energy. A small variation in any of these parameters can alter the $NB^{-\cdots}HA \leftrightarrow NBH^{\bullet\cdots} A^{-}$ equilibrium. For the proton transfer to occur, the stabilizing interaction in the $NBH^{\bullet\cdots} A^{-}$ system needs to: (i) compensate the barriers of hypothetical process:

$$NB^{-} + HA \rightarrow NBH^{\bullet} + A^{-} \qquad (21\text{-}1)$$

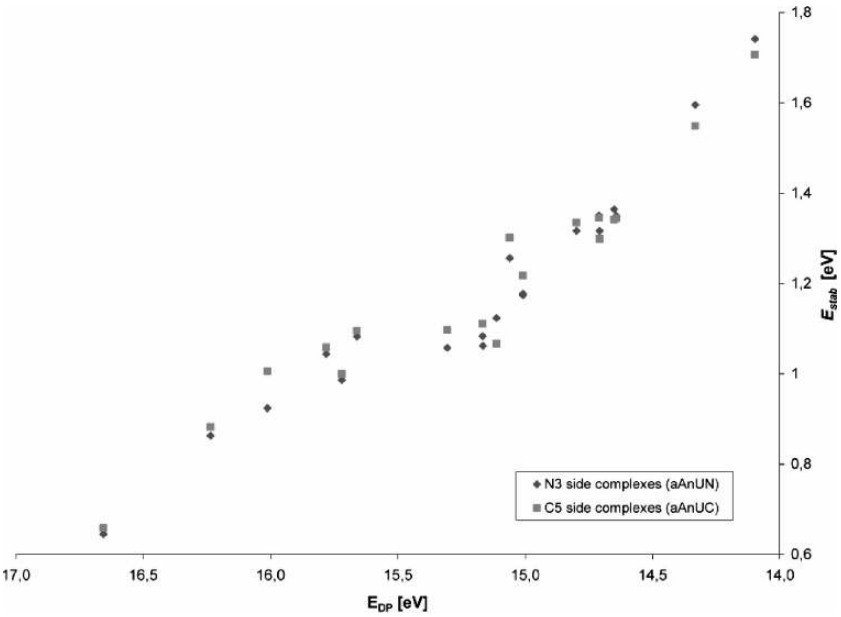

Figure 21-17. The stabilization energy (E_{stab}) in anionic uracil-alcohol complexes vs the deprotonation energy (E_{DP}) of ROH. All properties calculated at the B3LYP/6-31++G**(5d) level of theory (Figure 6 of ref. [48]. Reprinted with permission. Copyright 2005 American Chemical Society.)

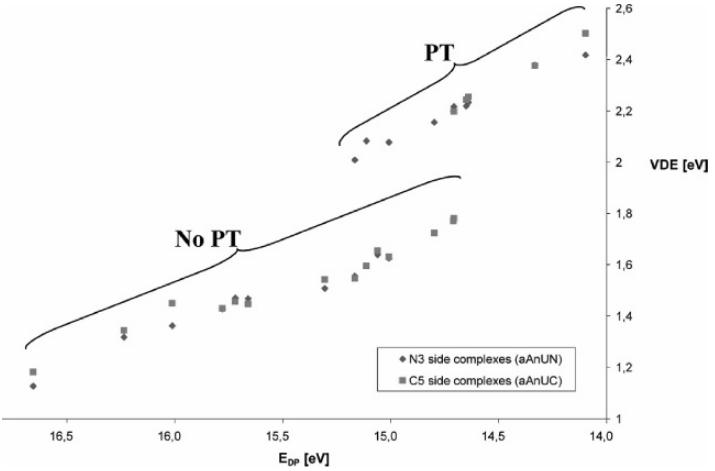

Figure 21-18. The vertical detachment energy in anionic uracil-alcohol complexes versus the energy of deprotonation of the alcohol. All properties calculated at the B3LYP/6-31++G**(5d) level of theory. "PT" and "No PT" are groups of complexes with and without proton transfer, respectively (Figure 5 of ref. [48]. Reprinted with permission. Copyright 2005 American Chemical Society.)

which leads to noninteracting products, (ii) provide at least as much of the stabilization between the $NBH^{\bullet}$ and A^{-} systems as the untransformed NB^{-} and HA moieties could provide.

For instance, a comparison of the photoelectron spectrum and computational data confirms that $[U\cdots HCN]^{-}$ does not undergo the intermolecular proton transfer. Indeed, the global minimum corresponds to the $U^{-}\cdots HCN$ complex. A position of the broad maximum of the photoelectron spectrum at 1.1–1.2 eV (Figure 21-19), and the estimated values of electron vertical detachment energies for the global minimum, which are 1.1 and 1.2 eV at the MP2 and B3LYP level, respectively, are consistent, thus confirming that only the $NB^{-}\cdots HA$ structure is present in the experiment. Similarly, the spectrum for the $[U\cdots H_2O]^{-}$ with the maximum of the main feature at 0.9 eV indicates the lack of BFPT. On the other hand, the most stable anionic $U\cdots H_2S$ complexes undergo BFPT, and the estimated values of VDEs are in the range of 1.88–1.97 eV, in agreement with the maximum of the photoelectron spectral peak at 1.9 eV (Figure 21-19). A hypothetical process (21.1) is unfavorable in terms of energy by 2.57 and 0.80 eV for uracil anion reacting with H_2O and H_2S, respectively. Such large difference in the value of the barriers, which have to be compensated for BFPT to proceed justifies the occurrence of the process in $[U\cdots H_2S]^{-}$ and lack thereof in $[U\cdots H_2O]^{-}$. However, the difference in the energy of reaction (21.1) for H_2S and HCN amounts to only 0.05 eV. Moreover, the barrier of reaction (21.1) favors BFPT in $[U\cdots HCN]^{-}$, whereas it is observed only for uracil complexes with H_2S (see Figure 21-19). Thus, we conclude that the hydrogen bonding in $[U\cdots HCN]^{-}$ fails to provide as much stabilization as in $[U\cdots H_2S]^{-}$ which emphasizes that the occurrence of BFPT results from a subtle interplay between

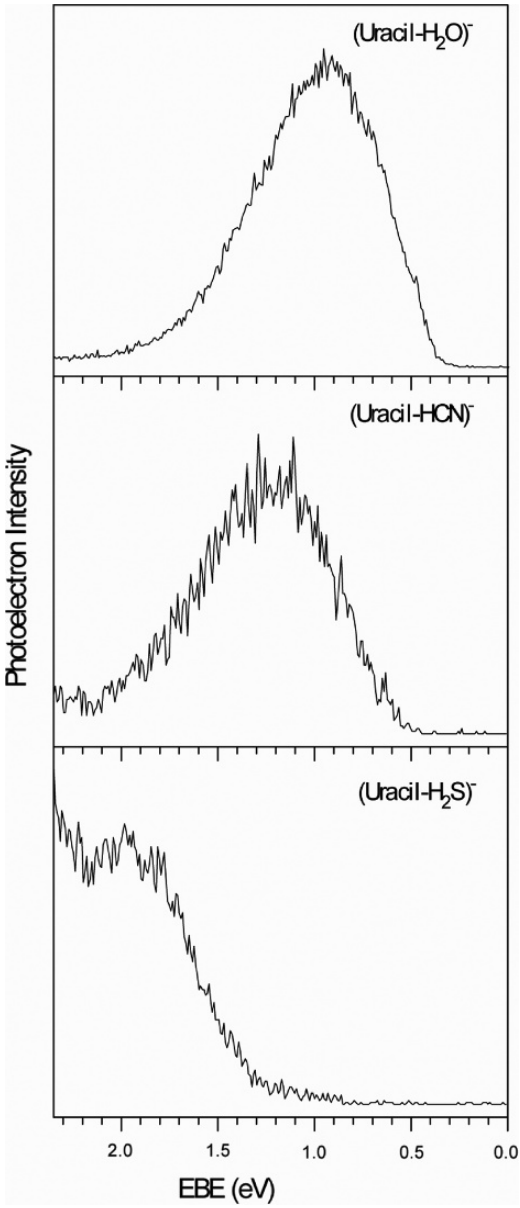

Figure 21-19. Photoelectron spectra of uracil-H_2O dimer anion (*top*), uracil-HCN dimer anion (*middle*), and uracil-H_2S dimer anion (*bottom*) recorded with 2.540 eV/photon. (Figure 7 of ref. [44]. Reprinted with permission.)

the deprotonation energy of HA, protonation energy of NB^- and the intermolecular stabilization energies in the $NB^{-}\cdots HA$ and $NBH^{\bullet}\cdots A^-$ systems.

21.2.3. BFPT in Binary Complexes of Nucleobases with Proton Donors

As was mentioned above the first system in which we discovered BFPT was the uracil-glycine complex [42]. The large difference of ca. 0.9 eV between the maxima in the PES spectra for the anions of $[U\cdots H_2O]$ and [U···glycine] (cf. the upper panel of Figure 21-19 with Figure 21-21a) cannot be attributed to the solvation of the intact glycine anion by uracil, since the most stable conformer of canonical glycine does not bind an electron, i.e. the measured EA of glycine is ca.−1.9 eV [55]. Theoretical results indicate that glycine forms only weakly bound anions with the VDE values, determined at the CCSD(T) level, of 0.083 eV for the canonical structure and 0.394 eV for the zwitterionic structure [56]. Thus, the electron binding energy shift induced by the interaction with uracil would have to be at least 1.4 eV to

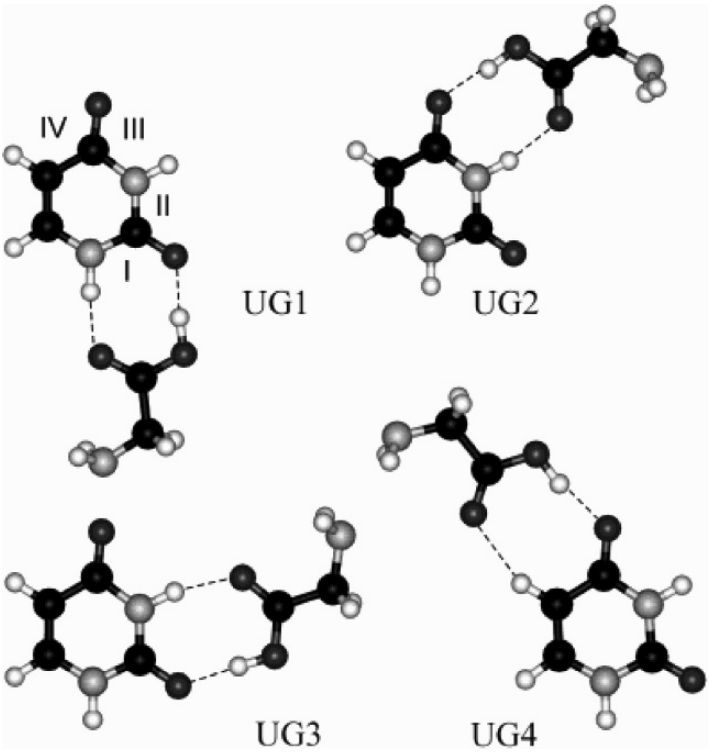

Figure 21-20. B3LYP/6-31++G** optimized structures of dimers UG1-UG4. I, II, III, and IV denote regions of the uracil monomer capable of forming two adjacent hydrogen bonds (Figure 2a of ref. [61]. Reprinted with permission. Copyright 2002 American Chemical Society.)

be consistent with the PES peak at 1.8 eV, which is improbable. Furthermore, at the CCSD(T) level of theory the valence anionic state of uracil is vertically stable with respect to the neutral by 0.506 eV [57]. And furthermore, the solvation of the uracil anionic state by one water molecule provides an extra stabilization of this state by ca. 0.4 eV [58, 59]. Thus, the solvation of U^- by the amino acid would have to provide an extra stabilization of 1.3 eV to be consistent with the maxima of the PES peaks at 1.8 eV, which is again improbable. This analysis prompted us to carry out computational studies comprising the possible uracil-glycine complexes stabilized by cyclic hydrogen bonds (i.e. by two hydrogen bonds). We searched over the conformational space of neutral complexes [60, 61] that allowed us to identify, at the B3LYP level [62–64] and with 6-31++G** basis set [65, 66] (B3LYP/6-31++G**), 23 complexes bound by two hydrogen bonds. The largest stabilization energy of 15.6 kcal/mol was determined for the UG1 structure [60, 61]. Two other low-energy structures, UG2 and UG3, are bound by 13.3 and 12.3 kcal/mol, respectively. Very similar stabilization energies were obtained at the MP2/6-31++G** level of theory. It turned out that the free energies of stabilization favor formation of uracil-glycine complexes for UG1, UG2, and UG3 only (for structures see Figure 21-20) [61].

The geometries of neutral complexes were, in turn, employed as starting structures in the geometry optimizations of valence anions. The excess electron induces a barrier-free proton transfer (the barrier-free nature of proton transfer has been confirmed at the MP2 level of theory) when the carboxylic group of glycine forms a hydrogen bond with the O8 atom of uracil. The driving force for the proton transfer is the stabilization of the negative excess charge localized primarily on the O8C4C5C6 position of uracil. The excess electron that occupies the π^* orbital localized at uracil induces buckling of its ring in order to diminish the antibonding effects (cf. the buckling of one of the formic acid molecule in formic acid dimer due to attachment of an excess electron, described in the previous section). The anionic complexes with the O8 site protonated are the most stable. These complexes can be viewed as the neutral radical of hydrogenated uracil solvated by the anion of deprotonated glycine and are characterized by the largest values of VDE, which span a range of 2.0–1.7 eV. These values of VDE were obtained by shifting the B3LYP values down by 0.2 eV, as suggested by the CCSD(T) results for the valence anionic state of an isolated uracil. A preference to transfer a proton to the O8 site is larger than to the O7 site, though some structures have been identified with the O7 site protonated. There are numerous structures of the neutral uracil glycine complexes, which do not undergo a barrier-free proton transfer upon attachment of an excess electron. These are primarily structures with glycine coordinated to the O7 atom. Some of these structures are the most stable among the neutral complexes [60, 61] but their favorable networks of hydrogen bonds cannot compensate for the unfavorable excess electron binding energies. The calculated vertical electron detachment energies for structures of this type are in a range of 0.9–1.5 eV and they may contribute to the relatively large width of the PES dominant peak (Figure 21-21).

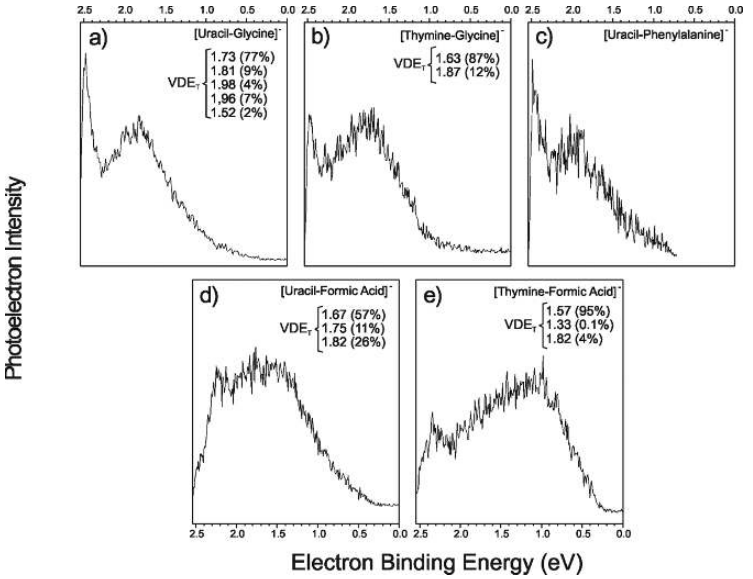

Figure 21-21. Photoelectron spectra of the dimer anions of: (a) uracil-glycine (Figure 2a of ref. [42]. Reprinted with kind permission of Springer Science and Business Media.), (b) thymine-glycine (Figure 2 of ref. [47]. Reprinted with permission of the PCCP Owner Societes.), (c) uracil-phenylalanine (Figure 2b of ref. [42]. Reprinted with kind permission of Springer Science and Business Media.), (d) uracil with formic acid (Figure 2 of ref. [45]. Reprinted with permission. Copyright 2004 American Chemical Society.), and (e) thymine-formic acid (Figure 2 of ref. [45] Reprinted with permission. Copyright 2004 American Chemical Society.). All spectra recorded with 2.540 eV photons. VDE_T stands for the theoretically predicted VDE value. All values of VDE are scaled down by 0.2 eV as suggested by CCSD(T) calculations. Displayed in parenthesis is the percentage fraction of a structure with given VDE_T in the equilibrated mixture of anions

A similar experimental-theoretical approach was used on other complexes comprising a pyrimidine nucleic base and proton donor. Here, one should mention the anions of nucleobase-amino acid complexes, uracil-phenylalanine [42], uracil-glycine [46] and thymine-glycine [47], the complexes of thymine and uracil with formic acid [45] as well as the above mentioned (see Section 21.2.3) complexes of uracil with inorganic acids such as H_2S, H_2Se and HCN [43, 44]. In all cases but the uracil···HCN anion, the lowest energy structure of anion turned out to be that resulted from BFPT. It is worth noting that the relative stability of complexes is different for the anionic and neutral structures. This emphasizes the need to consider both the neutral and the anionic potential energy surfaces in order to identify the most representative structures. Computationally predicted VDEs for the most stable geometries remain in a very good accordance with the maxima of main feature in the measured PES spectra (Figure 21-21).

Recently we have published the results of studies on BFPT induced by electron attachment in the binary complexes of adenine (A) and 9-methyladenine (MA)

with formic acid (FA) [67]. There is no experimental evidence for the occurrence of stable valence anions of bare adenine [33] and only computational results are available for anionic states of isolated adenine [68] and guanine [69, 70]. It is worth noting that the electron vertical attachment energy (VAE) of adenine measured using transmission electron spectroscopy assumes a substantial negative value of −0.794 eV [55]. The AEA for the formation of valence anions of uracil or thymine is close to zero while their VAEs are below −0.3 eV [55]. It implies that the AEA for the formation of a valence anion of adenine might be well below zero. The results of quantum chemical calculations fully account for this conclusion as only negative values of AEA have been found irrespective of the exchange-correlation functional and basis set used [33]. Thus, besides the experimental work of Desfrancois et al. [71], who reported that two molecules of water and three molecules of methanol are sufficient to stabilize the valence anion of adenine, all earlier reports indicated a significant instability of gas phase valence anions of adenine. Only dipole-bound anions were characterized in an earlier computational study by Jalbout and Adamowicz on $[A^{\cdots}(H_2O)_n]^-$ [72]. The results of the same authors on valence anions of $[A^{\cdots}(CH_3OH)_n]^-$ ($n \leq 3$) were inconclusive [73]. In contrast, all valence anions identified by us for A/MA$^{\cdots}$FA systems are adiabatically stable by 0.3–0.7 eV with respect to the neutral complexes. Hence, the stability of the [A/MA$^{\cdots}$FA]$^-$ complexes is dramatically enhanced by intermolecular proton transfer.

The theoretical data indicate that the excess electron in both $(AFA)^-$ and $(MAFA)^-$ occupies a π^* orbital localized on adenine/9-methyladenine and the adiabatic stability of the most anions amounts to 0.67 and 0.54 eV for AFA^- and $MAFA^-$, respectively [67]. The excess electron attachment to the complexes induces a barrier-free proton transfer (BFPT) from the carboxylic group of formic acid to a N atom of adenine or 9-methyladenine. As a result, the most stable structures of the anionic complexes can be characterized as neutral radicals of hydrogenated adenine(9-methyladenine) solvated by a deprotonated formic acid. The BFPT to the N atoms of adenine may be biologically relevant because some of these sites are not involved in the Watson-Crick pairing scheme and are easily accessible in the cellular environment. We suggest that valence anions of purines might be as important as those of pyrimidines in the process of DNA damage by low energy electrons.

While studying the AFA^- system in the manner described above we encountered a difficulty in reproducing its experimentally-determined VDE. The problem of calculating reliable VDE here has been traced back to the deficiency of the B3LYP method to predict correct geometries for some valence anions [67]. This effect is probably related to an artificial delocalization of the electronic charge predicted by the DFT methods [74]. Therefore, we built a statistical model which could correct the deficiency of the B3LYP method and render reliable estimates of VDE. In order to make this model general we used most of the experimental and theoretical data published for the BFPT systems. The proposed correlation equation for VDE depends on two parameters only. The first is the B3LYP value of VDE and the

second is the difference in non-planarity (ΔNP) of the nucleobase predicted at the B3LYP and MP2 levels. In each complex we determined the non-planarity of a nucleobase based on the geometry of its conjugated ring only. The NP is given by a sum of distances between heavy atoms in the ring and a plane determined by the same set of heavy atoms. The plane is determined in the standard least-squares procedure. In this way we ended up with the following equation:

$$VDE = a \bullet (\Delta NP)^2 + VDE(B3LYP) + b \tag{21-2}$$

where a and b are correlation coefficients. In this model an increase in the VDE value in comparison with the B3LYP result depends in a harmonic fashion on ΔNP. Since the model uses only the B3LYP and MP2 data it is much cheaper than the relatively accurate CCSD approach. Thus, the general recipe enabling a reliable estimation of VDE for this type of anions can be realized within a four-step procedure: (i) identification of the lowest energy anionic structure using an inexpensive B3LYP/6-31++G** model, (ii) re-optimization of this structure employing the MP2/aug-cc-pVDZ method, (iii) calculation of the difference in planarity between the B3LYP and MP2 structures, (iv) and finally the prediction of VDE using Eq. 21-2.

The theoretical-experimental studies on the complexes of a nucleobases with proton donor suggest that whenever a nucleobase interacts with a species of sufficient acidity the attachment of electron leads, usually via the BFPT process, to the formation of very stable valence anion. The excess electron localizes on the π^* orbital of a base inducing buckling of its ring and proton transfer from a proton donor to the heterocyclic atom of a nucleobase may take place. Such BFPT complexes can be viewed as the neutral radical of hydrogenated nucleobase solvated by the anion of deprotonated proton donor. Due to the number of proton donors accessible to a nucleobase incorporated in DNA (proteins interacting with DNA, other bases or molecules from DNA environment), the large adiabatic stability of the nucleobase···proton donor anions suggests that they might be involved in DNA damage by LEEs.

21.2.4. BFPT in the Anions of AT and GC Base Pairs

The BFPT process may take place whenever an excess electron is attached to a nucleobase interacting with a proton donor. In particular, the role of a proton donor could be filled by another nucleobase. Especially interesting are complementary base pairs, AT and GC, since these systems appear in DNA. In the case of the adenine-thymine base pair (AT), a combination of three proton donor and acceptor pairs of adenine with three proton donor and acceptor pairs of thymine leads to nine possible, planar, cyclic H-bonded complexes (see Figure 21-22 [49]).

A more suitable model, mimicking the DNA environment to a better extent, is the 9-methyladenine-1-methylthymine (MAMT) base pair, since in DNA nucleobases are bonded to deoxyribose (through the C-N bond) via these methylated positions.

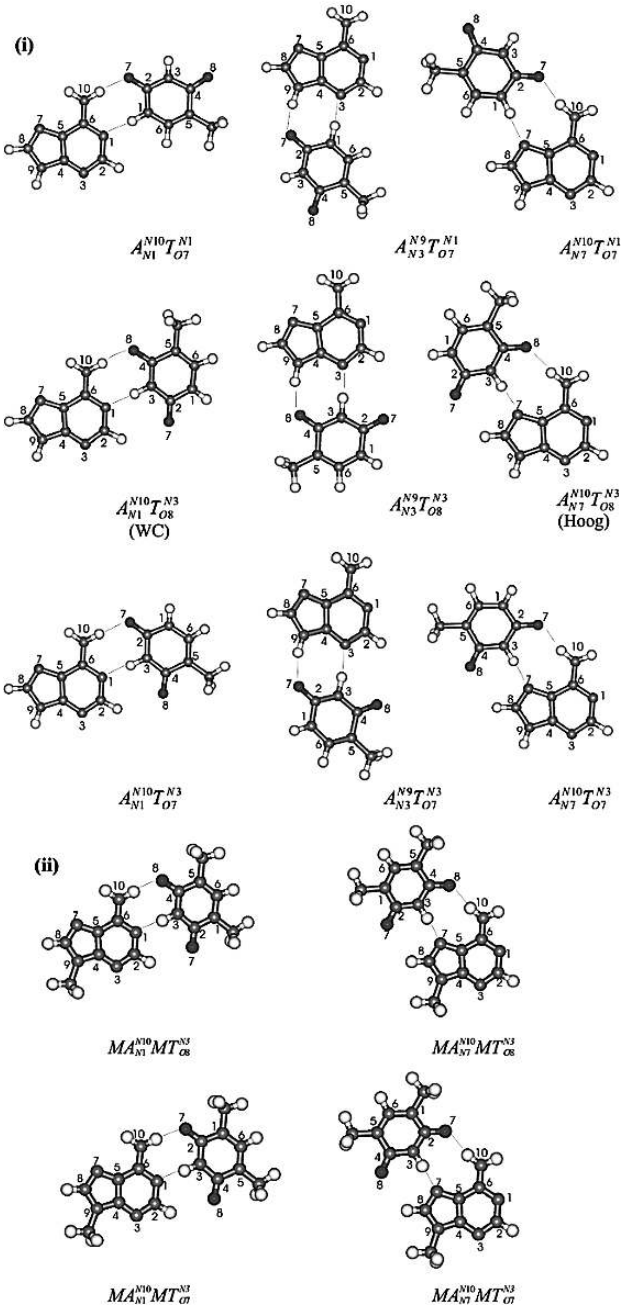

Figure 21-22. Optimized structures of neutral complexes of (i) adenine with thymine and (ii) 9-methyladenine with 1-methylthymine (Figure 1 of ref. [49]. Reprinted with permission. Copyright 2005 American Chemical Society.)

In Figure 21-22 the optimized structures of neutral MAMT complexes are also displayed. The photoelectron spectra of $(AT)^-$ and $(MAMT)^-$ recorded with 2.54 eV photons are shown in Figure 21-23. The vertical detachment energies of these two spectra are very different, their values being separated by about 1 eV. The photoelectron spectrum of $(AT)^-$ consists of a broad peak with maximum at ca. 1.7 eV, while the photoelectron spectrum of $(MAMT)^-$ consists of a broad peak with a maximum at ~0.7 eV (see Figure 21-23).

The global minimum on the anionic potential energy surface results from proton transfer from N9H of A to O8 of T (Table 21-1). A barrier that separates the global minimum from the non-PT structure is only 0.25 kcal/mol at the B3LYP/6-31+G** level of theory. This barrier is encountered on the surface of electronic energy, but it disappears on the surface of free energy, after inclusion of zero-point energies, thermal energies, and the entropy terms. The PES spectrum will be dominated by contributions from the most stable AT^- structures (see Table 21-1 and Figure 21-23) with the corresponding VDE values of 1.3 and 2.0 eV. Indeed, the maximum of the PES spectrum is at 1.7 eV, in agreement with the calculated values of the VDE.

The most stable anionic complexes for methylated bases correspond to the Hoogsteen and Watson-Crick structures, with the former being more stable by 2.0 and 1.2 kcal/mol in terms of ΔE and ΔG, respectively; see Table 21-1 and Figure 21-22. Both structures are characterized by a VDE of ca. 0.8 eV at the

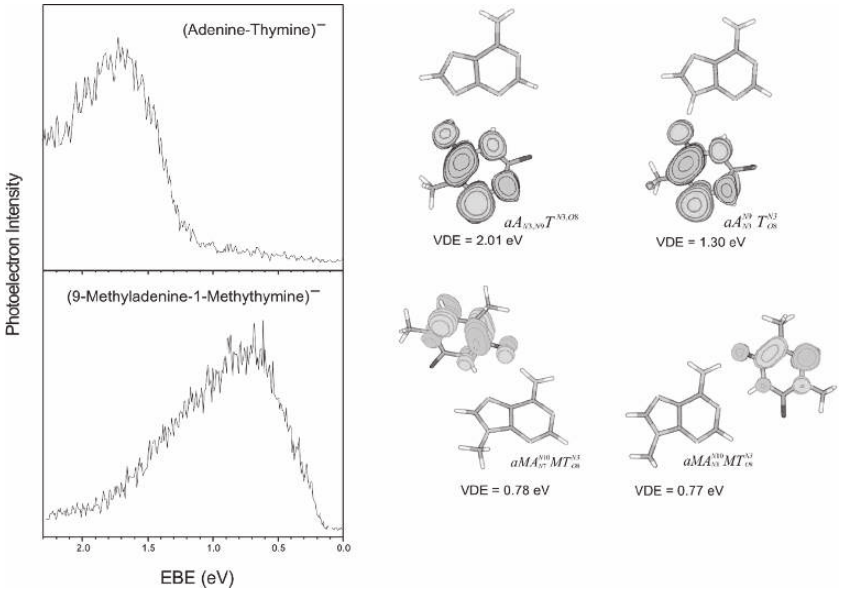

Figure 21-23. Unpaired electron orbital plotted with a contour line spacing of 0.03 bohr-3/2 for the two most stable anions of (i) AT pair and (ii) MAMT pair (Figure 2 of [49]. Reprinted with permission. Copyright 2005 American Chemical Society.)

Table 21-1. Values of stabilization energy (E_{stab}), stabilization free energy (G_{stab}), their relative values (ΔE and ΔG calculated with respect to the Watson-Crick pair), electron vertical detachment energy (VDE) and adiabatic electron binding energy (EBE_G) for the anionic adenine–thymine and 9-methyladenine-1-methylthymine complexes calculated at the B3LYP/6-31+G** level. (Table 1 of ref. [49]. Reprinted with permission. Copyright 2005 American Chemical Society.)

Structure	E_{stab}	ΔE	G_{stab}	ΔG	EBE_G	VDE
			T_{O8}^{N3} family			
$aA_{N3}^{N9}T_{O8}^{N3}$	−22.85	−7.39	−11.11	−8.42	14.65	1.30
$aA_{N3,N9}T^{N3,O8}$	−23.89	−8.43	−11.07	−8.39	14.62	2.01
$aA_{N7}^{N10}T_{O8}^{N3}$	−17.52	−2.06	−3.86	−1.18	9.18	0.91
$aA_{N1}^{N10}T_{O8}^{N3}$	−15.46	0	−2.68	0	8.66	0.89
			T_{O7}^{N1} family			
$aA_{N3}^{N9}T_{O7}^{N1}$	−20.24	−4.78	−8.52	−5.84	10.14	0.52
$aA_{N7}^{N10}T_{O7}^{N1}$	−16.11	−0.65	−4.17	−1.49	9.55	0.33
$aA_{N1}^{N10}T_{O7}^{N1}$	−15.53	−0.07	−3.46	−0.78	7.96	0.26
			T_{07}^{N3} family			
$aA_{N3}^{N9}T_{O7}^{N3}$	−17.46	−2.0	−4.90	−2.22	8.68	1.03
$aA_{N7}^{N10}T_{O7}^{N3}$	−14.80	0.66	−0.93	1.75	6.40	0.80
$aA_{N1}^{N10}T_{O7}^{N3}$	−11.95	3.52	0.48	3.16	5.68	0.61
			9-methyladenine-1-methylthymine MT_{O8}^{N3} family			
$aMA_{N7}^{N10}MT_{O8}^{N3}$	−16.72	−1.97	−3.66	−1.18	8.17	0.78
$aMA_{N1}^{N10}MT_{O8}^{N3}$	−14.76	0	−2.48	0	7.69	0.77
			MT_{O7}^{N3} family			
$aMA_{N7}^{N10}MT_{O7}^{N3}$	−14.00	0.75	−0.90	1.58	5.58	0.69
$aMA_{N1}^{N10}MT_{O7}^{N3}$	−11.20	3.55	−0.37	2.11	5.93	0.41

[a] E_{stab}, G_{stab}, ΔE, ΔG, and EBE_G are in kilocalories per mole; VDE is in electron volts.

B3LYP/6-31+G** level. The results are consistent with the maximum of the PES peak for $MAMT^-$ at 0.7 eV (Figure 21-23).

The employed computational methodology allowed us to explain the PES spectra of AT^- and $MAMT^-$ in the gas phase. Simultaneously, we demonstrated that PT induced by electron attachment, important for the unconstrained AT complexes, is irrelevant for the biologically essential Watson-Crick configuration as modeled by the MAMT complex. Nevertheless, the Watson-Crick MAMT structure binds an excess electron that localizes on thymine, by 7.7 kcal/mol (see structure $aMA_{N1}^{N10}MT_{O8}^{N3}$ in Table 21-1 and Figure 21-23).

The anionic Watson-Crick guanine-cytosine base pair behaves in a different manner [75]. Namely, out of several possible configurations, differing with the position of proton(s), the geometry with proton transferred from the N1 atom of guanine to the N3 atom of cytosine turned out to be the global minimum. This structure is more stable than the Watson-Crick anion by 2.9 (B3LYP) and

5.6 (RI-MP2) kcal/mol [75], and is adiabatically stable with respect to the neutral GC configuration by 11.7 and 12.3 kcal/mol [75], in terms of electronic energy, predicted at the B3LYP/6-31++G** and RI-MP2/aug-cc-pVDZ levels, respectively (Figure 21-24). The Watson-Crick GC configuration is separated from the PT geometry by a small kinetic barrier of 2.6 and 1.3 kcal/mol in the electronic energy scale, calculated at the B3LYP and RI-MP2 level, respectively (Figure 21-24).

At the ambient temperature barrier of that size is easily overcome and, therefore, attachment of excess electron to the GC base pair (incorporated in DNA as the Watson-Crick configuration) should end up with the neutral radical of hydrogenated cytosine solvated by the anion of deprotonated guanine. Proton transfer induced by electron attachment has already been suggested in the past by the group of Sevilla within their computational [76] and experimental studies [77].

21.2.5. Interactions of DNA with Proteins and Proton Transfer Induced by Excess Electrons

The DNA damage process is thought to begin with anionic states localized on pyrimidine bases and, accordingly, all theoretical studies concerning the breakage mechanism have focused on pyrimidine bases or their nucleotides [29, 36, 78–80]. This supposition is based on the electron affinities of isolated nucleobases. Indeed, the adiabatic gas-phase electron affinities of the valence anions of canonical tautomers of nucleic bases, calculated at the B3LYP/DZP++ level, diminish in the following sequence [81]: U>T>C>G>A, and for pyrimidines compare very well with the values extrapolated from photoelectron spectra of nucleobase•$(H_2O)_n$ clusters [82]. This AEA sequence therefore suggests that thymine and cytosine molecules are primary targets for the formation of nucleic base anions in DNA. One should, however, realize that in contrast to pyrimidine bases, purine molecules possess proton-donor and -acceptor centers that are not involved, or only partially involved, in the Watson-Crick (WC) pairing scheme, and may therefore form

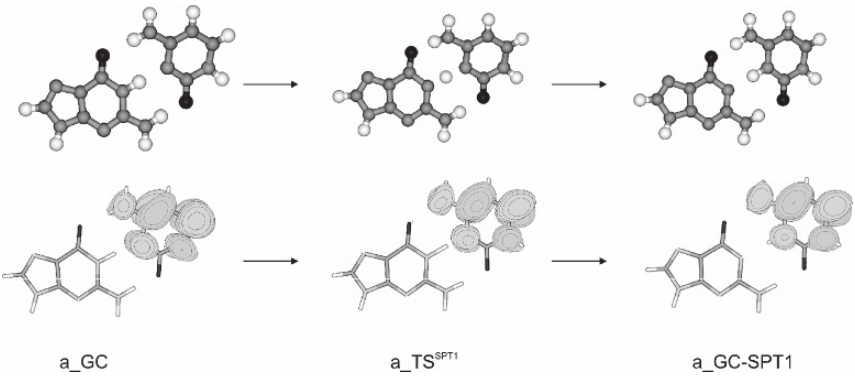

Figure 21-24. Proton transfer induced by electron attachment in the GC Watson-Crick base pair [75]

additional hydrogen bonds (HBs), e.g., in the Hoogsteen pairing scheme [83]. Hence, the interaction between anionic purines and amino acid side chains (e.g. due to interaction between DNA and histones, and repair or replication enzymes) might counterbalance the larger EAs of free pyrimidines. If so, then both types of nucleobases could play a significant role in DNA damage induced by low-energy electrons. We inspected interactions published in an amino acid-nucleotide database (AANT) containing crystallographic structures for 1213 protein-nucleic acids complexes [84] and observed that the purine-amino acid side chains contacts account for the majority of interactions. Namely, out of 3066 contacts between nucleobases and amino acid side chains 43.7 and 21.4% fall to guanine and adenine, respectively. As was demonstrated [50], the presence of formic acid renders the valence anion of adenine and 9-methyladenine exceptionally stable.

In the cellular environment guanine may interact for example with the side chain of arginine, which at the physiological pH is protonated. Indeed the analysis of the AANT database indicates that the Hoogsteen type interactions between guanine and charged arginine account for the majority of guanine-amino acid side chain contacts. Attachment of an electron to guanine complexed with charged arginine might induce BFPT (similar to the BFPT predicted in the anions of AFA and MAFA). Moreover, the reactive neutral AH radical abstracting a hydrogen atom from deoxyribose might initiate a sequence of processes leading to a single strand break [9].

Very recently we have systematically studied the effects of possible hydrogen bonding interactions between amino acid side-chains and nucleotide base pairs on VDEs of respective complexes [85, 86]. The possible systems were assumed after Cheng et al. [87], who predicted geometrically plausible arrangements that were, indeed, observed in the crystal structure of complexes between proteins and nucleic acids. The results of our B3LYP/6-31+G** calculations indicate that interactions of guanine from the GC base pair with the arginine or lysine residue enables formation of anions with the excess electron localized entirely on guanine and with AEAs that amount to as much as 3.4 eV [85].

In a study concerning the AT base pair interacting with a series of organic acids ((HX)AT) via Hoogsteen-type hydrogen bonds [88] with adenine we, indeed, demonstrated that higher EA of pyrimidine nucleotides might be counterbalanced by purine base-proton donor interactions. We employed the Hoogsteen-type arrangement for the organic acid-adenine interaction (Figure 21-25) since the N7 and N10 atoms of adenine are exposed to the environment of the major groove of B-DNA, the favored site of nucleobase interactions with external agents [89].

The attachment of an electron to these trimers is thermodynamically feasible and, depending on the HX acid, leads to three or two anionic structures. In all the systems studied, electron attachment is accompanied by proton transfer, with (PT) or without a small kinetic barrier (BFPT), from the carboxylic group of the acid to atom N7 in the five-membered ring of adenine. In the BFPT systems only single- and double-PT anions are produced. For the remaining complexes an anion having the structure of the intact HX(AT) complex was identified in addition to the single- and

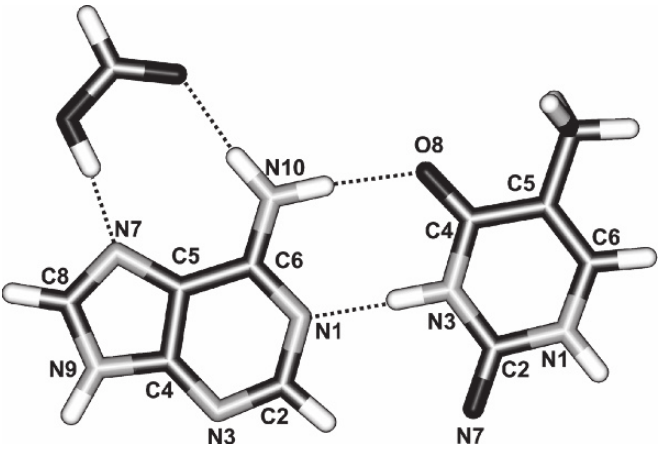

Figure 21-25. Nucleobase atom numbering for the FA(AT) trimer (Figure 1 of ref. [88])

double-PT anionic configurations. The AEA's calculated at the B3LYP/6-31+G** level assume significantly positive values that vary between 0.41 and 1.28 eV (Table 21-2). Vertical detachment energies for the non-PT anions assume values in the narrow range of 0.36–0.39 eV, whereas for the BFPT structures they are much larger and scattered, spanning the range from 1.71 to 2.88 eV (Table 21-2). As indicated by the SOMO distribution in the non-PT structures the excess electron is delocalized over thymine and adenine, while in all PT anions it is entirely localised on adenine.

Table 21-2. Relative electronic energies and free energies (ΔE and ΔG) calculated with respect to the aHX(AT) or aHX(AT)-SPT anion together with the adiabatic electron affinities (AEA_G) and electron vertical detachment energies (VDE) for the anionic HX(AT) complexes predicted at the B3LYP/6-31+G** level. ΔE and ΔG in kcal/mol; AEA_G and VDE in eV

Anion[a]	ΔE	ΔG	AEA_G	VDE
aFA(AT)	0	0	0.47	0.39
aFA(AT) – SPT	−4.26	−2.45	0.57	1.78
aFA(AT) – DPT	−4.88	−1.31	0.58	2.36
aAA(AT)	0	0	0.41	0.36
aAA(AT) – SPT	−2.33	−1.04	0.45	1.71
aAA(AT) – DPT	−3.15	−2.57	0.47	2.29
aClFA(AT) – SPT	0	0	1.28	2.04
aClFA(AT) – DPT	1.63	2.15	1.19	2.88
aFFA(AT) – SPT	0	0	1.03	2.09
aFFA(AT) – DPT	0.55	0.98	0.99	2.65

[a] FA, AA, ClFA, FFA and AT stands for HCOOH, CH_3COOH, ClCOOH, FCOOH and the Watson-Crick adenine-thymine base pair, respectively, whereas SPT and DPT indicates single- and double-proton transfer structures, respectively.

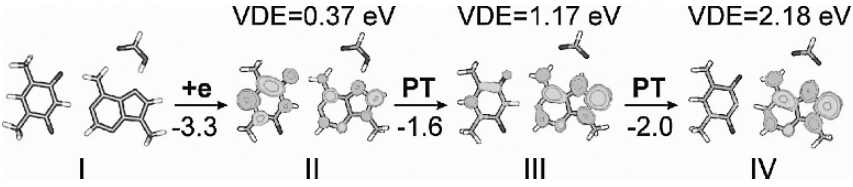

Figure 21-26. Electron binding to the Watson-Crick MAMT base pair solvated by formic acid at the Hoogsteen site (I). In consequence of intermolecular proton transfers the radicals $MAH^{\bullet}$ (III) and $MAH_2^{\bullet+}$(IV) are formed and the unpaired electron becomes localized on 9-methyladenine. Both initial electron attachment and two following intermolecular proton transfers are thermodynamically favourable and the accompanying changes of B3LYP electronic energies are given below the arrows in kcal/mol (Figure 7 of ref. [67]. Reprinted with permission. Copyright 2007 American Chemical Society.)

A systematic computational and experimental study on the anionic 9-methyladenine-1-methylthymine-formic acid trimer, $MAMTFA^{-}$, leads to similar conclusion [90]. In Figure 21-26 a hydrogen bonded system, in which the Watson-Crick MAMT pair forms a cyclic hydrogen bonded structure with FA through the Hoogsteen sites of MA, i.e., N7 and N10H is shown. The excess electron attachment to this trimer leads to an anionic structure with an unpaired electron localized primarily on thymine and characterized by a VDE of 0.37 eV. This localization of the unpaired electron is consistent with the sequence of electron affinities of isolated NBs: T>A [81]. The anionic structure is, however, only a local minimum on the potential energy surface of the anionic trimer. The values of proton affinities and deprotonation enthalpies for the relevant sites of neutral adenine and thymine suggest that intermolecular proton transfer from thymine to adenine is feasible. Indeed, two consecutive intermolecular proton transfers are thermodynamically favorable and lead to: (1) an intermediate anionic trimer built of $MAH^{\bullet}$, deprotonated FA, and MT, and (2) the global minimum structure built of $MAH_2^{\bullet+}$, deprotonated FA and deprotonated MT. In consequence of two intermolecular proton transfers, the excess electron is localized exclusively on adenine and the VDE is as large as 2.18 eV.

These results suggest, thus, that environment-DNA interactions could counterbalance or even reverse the experimentally observed stability of isolated nucleic base anions. As a consequence, the delocalization of an electron over the Watson-Crick base pair could initiate CX-O bond breakage from either a pyrimidine or a purine anion.

21.3. MECHANISMS OF SSB FORMATION IN DNA

21.3.1. Nonadiabatic Through Bond Electron Transfer Involving Resonances of Pyrimidine Bases

The unexpected discovery that very low energy electrons are able to cleave bonds in DNA [12] aroused a great deal of interest within radiation research community [1, 2]. The most obvious mechanistic proposal explaining the observed DNA damage

involved attachment of an electron to a phosphate group. Indeed, direct attachment of near zero energy electrons to the phosphate group leading to the cleavage of the C3′-O or C5′-O σ bond was studied theoretically by Li et al. [91]. However, according to the work of Berdys et al. [92, 93], zero energy electrons may not easily attach directly to the phosphate units as implied in the work of Li et al. [91]. Direct electron attachment can, indeed, produce a metastable P = O π^* anion, but this process would require electrons with energy larger than 2 eV.

Taking into account experimental data which suggested a resonance character of the damage process (the resonance type of the process is indicated by the shape of the damage yield function), the group of Simons proposed, using the HF/6−31+G* level of theory, a DNA damage mechanism based on electron transfer from a π^* shape resonance of a given nucleic acid base [29]. They assumed that an electron attaches to the lowest π^*-orbital of cytosine or thymine and within through-bond electron transfer process, cleaves the sugar-phosphate C-O σ-bond. They evaluated the rates of SSB formation using a Boltzmann-type model (see Eq. 21-3). Namely, they obtained those rates by multiplying the C-O vibrational frequency (assuming it to be equal ca. 10^{13} s^{-1}) by the equilibrium Boltzmann probability that the C-O bond is stretched enough (either before or after electron attachment) to reach the barrier (of height E^*).

$$P = \frac{e^{\frac{-E^*}{kT}}}{q} \tag{21-3}$$

The symbol q in Eq. 21-3 is the vibrational partition function for the C-O stretching mode. The barrier heights, E*, found when electrons are attached to cytosine or thymine ranged from 0.2 to 1 eV [29]. As a result, the estimated C-O bond cleavage rates range, at 298 K, from 10^{10} to 10^{-4} s^{-1}. Because the autodetachment rate of a π^* shape resonance is expected to be near 10^{14} s^{-1}, these bond cleavage estimates suggest that at most 1 in 10^4 nascent π^* anions should undergo C-O bond rupture. The rates of SSBs formation predicted in the manner described above are much slower than the rates at which the attached electron undergoes nonadiabatic through-bond transfer, and, therefore, according to the Simons group [29], it is these "Boltzmann" rates that limit the rates of SSB formation.

The bottleneck of very short lifetimes of resonace states (10^{-14} s) becomes less severe once one assumes that the primary role of resonance states is to provide doorways to bound valence anionic states, with lifetimes determined by kinetics of the following chemical reactions [36]. The reactions might proceed on these regions of potential energy surfaces, at which valence anions are bound with respect to the neutral species. The rates of these chemical transformations, e.g., the SSB formation, do not have to compete with short lifetimes of resonance states. It is worth noting that even for a kinetic barrier of ca. 20 kcal/mol, the half lifetime amounts (at 298 K) to about 30 seconds. Hence, if the kinetic barrier for SSB formation were lower than 20–23 kcal/mol, all nucleotides that could form stable anions would have enough time to cleave the C-O bond on the timescale of the electrophoretic assay of DNA damage.

21.3.2. Formation of Single Strand Breaks via Adiabatically Stable Anions of Pyrimidine Nucleotides

Very recently a proposal for SSB formation based on adiabatically stable anions localized on nucleobases has been published by the Leszczynski group [79, 80]. In their mechanism electrons attach to the DNA bases, forming the base-centered radical anions of the nucleotides in the first step of the cleavage process. Then, these electronically stable radical anions undergo C-O bond breaking and yield neutral ribose radical fragments and corresponding phosphate anions (Figure 21-27).

With the reliably calibrated B3LYP/DZP++ approach [94], the electron affinity of 3′-dCMPH (electron attachment to 3′-dCMPH leads to the base-centered radical anion in the first step of the assumed mechanism) has been studied by Schaefer and coworkers [95]. This investigation revealed that 3′-dCMPH was able to capture a near 0 eV electron to form a stable radical anion in both the gas phase and an aqueous solution. Thus, this pyrimidine-based radical anion is electronically stable enough to undergo the subsequent phosphate–sugar C-O bond-breaking or the glycosidic bond cleavage. Positive electron affinity was also confirmed for the remaining 3′- and 5′-monophospathes of pyrimidine nucleotides (Table 21-3).

It is worth noting that interaction with solvent remarkably increases the propensity of nucleotides to bind an electron. For instance, in the formation of the 5′-dCMPH radical anion, the AEA and VEA values in water are increased by 1.69 and 1.51 eV, respectively, with respect to the gas phase values (see Table 21-3). The solvent effects also significantly increase the electronic stability of the 5′-dCMPH radical. The VDE of 5′-dCMPH$^-$ in an aqueous solution is predicted to be 2.45 eV (1.69 eV larger than in the gas phase). A similar tendency was revealed for the remaining nucleotides (Table 21-3).

In Table 21-4 the relative thermodynamic characteristics for stationary points along the reaction path leading from the base-center radical anion to the products of the C-O bond cleavage are gathered. The activation energies for the CX′-O bond cleavage are relatively low. They are especially favorable for the bond rupture proceeding in the 3′-phosphates, i.e. 6.2 and 7.1 kcal/mol for 3′-dCMPH$^-$ and 3′-dTMPH$^-$, respectively (Table 21-4). Since the activation energy needed for the N1-glycosidic bond breaking in the anion is much higher than that for the rupture of the CX′-O bond (for instance, in dC$^-$ the barrier for the glycosidic bond dissociation

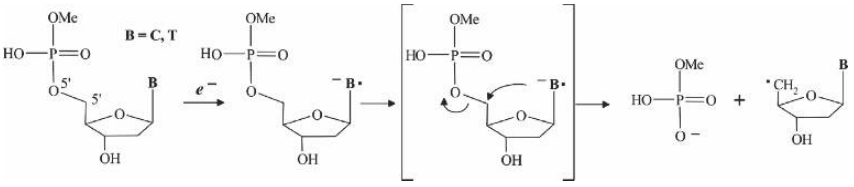

Figure 21-27. Proposed mechanism of the LEE-induced single-strand bond breaking in pyrimidine nucleotides (Scheme 2 of ref. [79]. Reprinted with permission. Copyright (2006) National Academy of Sciences, USA)

Table 21-3. Electron affinities of monophosphates of thymidine and cytidine (in eV). The values with zero point correction are given in parentheses (Table 1 of ref. [79] (Reprinted with permission. Copyright (2006) National Academy of Sciences, U.S.A.) and Table 1 of ref. [80] (Reprinted with permission. Copyright 2006 American Chemical Society.))

Electron attachment process	EA_{ad}	VEA[a]	VDE[b]
	Gas phase		
3′-dCMPH → 3′-dCMPH$^-$	0.33 (0.44)	0.15	1.28
3′-dTMPH → 3′-dTMPH$^-$	0.44 (0.56)	0.26	1.53
5′-dCMPH → 5′-dCMPH$^-$	0.20 (0.34)	−0.11	0.85
5′-dTMPH → 5′-dTMPH$^-$	0.28 (0.44)	0.01	0.99
	Aqueous solution (PCM [97], ε = 78.4)		
3′-dCMPH → 3′-dCMPH$^-$	2.18	1.72	2.97
5′-dCMPH → 5′-dCMPH$^-$	1.89	1.40	2.45
5′-dTMPH → 5′-dTMPH$^-$	1.96	1.53	2.60

[a]VEA = E(neutral) − E(anion); based on the optimized neutral structures. [b]VDE = E (neutral) – E (anion); based on the optimized anion structures.

Table 21-4. The relative electronic energies (ΔE_r) and free energies (ΔG_r^0) at 298 K of stationary points on the reaction path leading from the radical anions (Y′-dXCMPH$^-$; Y′ = 3′,5′, X=C,T) via transition states (TS) to the C3′-O and C5′-O bond broken complexes (Product complex) for electron induced dissociation of pyrimidine nucleotides. All values given in kcal/mol. (Table 2 of ref. [79] (Reprinted with permission. Copyright (2006) National Academy of Sciences, U.S.A.) and Table 1 of ref. [80] (Reprinted with permission. Copyright 2006 American Chemical Society.))

Species	ΔE_r^a	ΔG_r^0
5′-dCMPH$^-$	0.0	0.0
$TS_{5'-dCMPH-}$	14.27 (17.97)	12.75
Product complex (5′-dCMPH$^-$)	−22.97(−19.19)	−25.97
5′-dTMPH$^-$	0.0	0.0
$TS_{5'-dTMPH-}$	13.84 (17.86)	11.82
Product complex (5′-dTMPH$^-$)	−21.01(−16.05)	−23.19
3′-dCMPH$^-$	0.0	0.0
$TS_{3'-dCMPH-}$	6.17 (12.82)	4.54
Product complex (3′-dCMPH$^-$)	−20.81(−19.65)	−24.43
3′-dTMPH$^-$	0.0	0.0
$TS_{3'-dTMPH-}$	7.06 (13.73)	4.42
Product complex (3′-dTMPH$^-$)	−20.22(−17.84)	−23.70

[a] values obtained at the level of polarizable continuum model (PCM) with ε = 78.39 given in parentheses.

amounts to 21.6 kcal/mol, which is 7.3 kcal/mol more than the energy required for the C5′-O bond cleavage in 5′-dCMPH$^-$ [96]), the N1-glycosidic bond rupture is unlikely to compete with the breakage of the phosphodiester bond.

The presence of water, accounted for at the self-consistent reaction field level (PCM) [97], raises the CX′-O bond-breaking energy barrier. Namely, in water this barrier amounts to 18.0 and 17.9 kcal/mol for 5′-dCMPH$^-$ and 5′-dTMPH$^-$, respectively, and to 12.8 and 13.7 kcal/mol for 3′-dCMPH$^-$ and 3′-dTMPH$^-$, respectively. As a consequence, the half-lifes of respective anions range from 2×10^{-4} to 1×10^{0} s at 298 K. Simultaneously, the thermodynamic stimulus for the scission reaction assumes extremely favorable values of −25.97, −23.19, −24.43, and −23.70 kcal/mol for 5′-dCMPH$^-$, 5′-dTMPH$^-$, 3′-dCMPH$^-$, and 3′-dTMPH$^-$, respectively (Table 21-4). Hence, the 1–3 hour period usually required for the electrophoretic assay of SBs in DNA is sufficient for the cleavage process to be completed.

An analysis of the singly occupied molecular orbitals (SOMOs) provides insights into the electron attachment and the bond breaking mechanisms. Figure 21-28 illustrates the distribution of the unpaired electron along the LEE-induced C5′-O bond-breaking pathway for 5′-CMPH. The SOMO of the radical anion at the geometry of the neutral (first point on the reaction path) partly displays a dipole bound character (Figure 21-28). After structural relaxation, the excess electron localizes on the π^* orbital of the base, forming adiabatically stable valence radical anion (Tables 21-3 and 21-4). The antibonding character of the C5′-O interaction can be clearly recognized in the SOMO of the transition state (Figure 21-28). The examination of SOMO in TS for C3′-O cleavage explains the lower value of activation energy compared to the rupture of C5′-O. Namely, it reveals that excessive charge on the base facilitates an attack on C3′ from the back side of the phosphate leaving group. This resembles the nucleophilic S_N2 mechanism. The migration of negative charge from the base to the C3′-O bond proceeds directly through the atomic orbital overlap between the C6 atom of pyrimidine and the

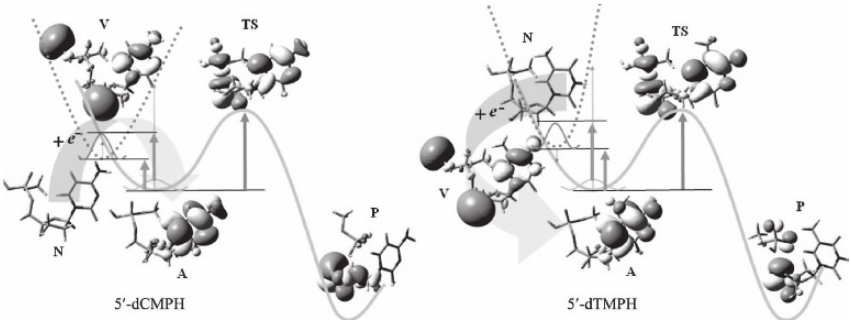

Figure 21-28. The distribution of the unpaired electron along the LEE-induced C5′-O bond-breaking pathway of the nucleotides (Figure 2 of ref. [79]. Reprinted with permission. Copyright (2006) National Academy of Sciences, USA.)

C3′ center of deoxyribose. Due to stereochemical reasons a similar configuration cannot be realized in the 5′-phosphates of pyrimidines. Finally, the distribution of SOMO in the CX′-O fragments indicates that the radical resides on the CX′ atom of deoxyribose moiety and consequently the excessive charge is localized on the phosphate group (Figure 21-28).

Very recently this damage mechanism has been questioned by Kumar and Sevilla [98], who claim that the barrier for the C5′-O bond scission in 5′-CMPH$^-$ in aqueous environment is so high that the proposed pathway will not significantly contribute to bond cleavage. However, their model of solvation was based only on scattered crystallographic data and chemical intuition. In our opinion, to obtain sound results concerning such a sensitive characteristic as activation energy (within a model explicitly describing the reactant and solvent molecules) one should carry-out hybrid molecular dynamics/quantum mechanics calculations. The activation barrier should strongly depend on the arrangement of water molecules in the solvation shell. The conformational space of any complex comprising a nucleotide anion and several ($\geq$5) water molecules is huge and without a thorough search for the global minimum (the case of studies described in ref. [98]) the result could be accidental.

21.3.3. Two-Electron Mechanisms of DNA Damage Triggered by Excess Electrons

A markedly different proposal for the DNA cleavage mechanism (from that reported by Leszczynski's) group was published by us in 2005 [36]. To the best of our knowledge this was the first mechanism presented in the literature for single strand break formation to be based on the formation of stable valence anions of nucleobases. Figure 21-29 displays the main idea of our suggestion for the C3′-O bond scission in 3′-phosphate of cytidine.

In the first stage, the nucleic acid base (within a nucleotide) is hydrogenated at the N3 position forming (Cy+H)$^\bullet$. The (Cy+H)$^\bullet$ intermediate can be formed in at least two ways: (a) excess electron attachment to the base followed by an intermolecular proton transfer, or (b) as a direct attachment of the hydrogen atom. In the first case, an electron-induced proton transfer may develop, without or with a very small barrier, whenever an anionic nucleic base interacts with proton donors, such as weak acids (see Section 21.2.2) or the complementary nucleic acid base; e.g., the intermolecular proton transfer occurs in the anionic Watson-Crick GC pair [75, 99, 100]. In the case of direct hydrogenation we anticipate two possible sources of hydrogen radicals: from surrounding water (water radiolysis) or from neighbouring NB's (DEA). In the second stage of the proposed mechanism, an electron is captured by the radical of a hydrogenated base and a closed-shell anion (Cy+H)$^-$ is formed. The electron vertical detachment energy for the anion is significant, ca. 32 kcal/mol, and the anion is adiabatically bound by 12 kcal/mol (B3LYP/6-31++G** result). The excess negative charge is formally localized on the C6 atom of Cy but it also spreads over the C4-C5 area.

At the third and critical stage of the proposed mechanism, a proton is transferred from the adjacent sugar to the negatively charged C6 atom of $(Cy+H)^-$. The MPW1K/6−31+G** [101] barrier for proton transfer from the C2′ atom of sugar to C6 of $(Cy+H)^-$ is 5.6, 3.4, and 4.2 kcal/mol in terms of electronic energy, electronic energy corrected for zero-point vibrations, and Gibbs free energy, respectively (the MPW1K functional was specifically designed to reproduce barrier heights of chemical reactions). The proton transfer leads formally to a product, in which the negative charge is localized on the sugar unit. In our calculations, however, we could not identify the product of step (3) (Figure 21-29). Instead we observe a spontaneous, barrier-free cleavage of the C-O sugar-phosphate bond leading to the product with the negative charge localized on the phosphate unit.

The CH stretching frequency is at ca. 3000 cm^{-1}, which corresponds to a rate of vibration of 8.9×10^{13} s^{-1}. The Boltzmann's probability for surmounting the 4.2 kcal/mol barrier at T = 298 K is 8.3×10^{-4}. Thus, the average rate of strand

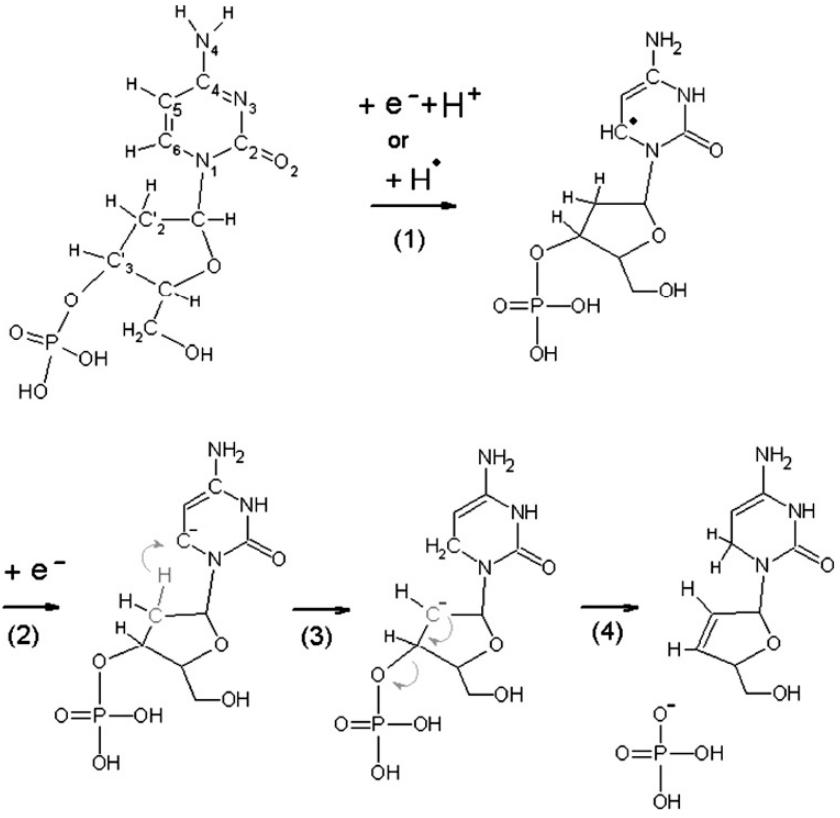

Figure 21-29. Proposed two-electron mechanism of the DNA strand break induced by excess electrons (Figure 1 of ref. [36]. Reprinted with kind permission of Springer Science and Business Media.)

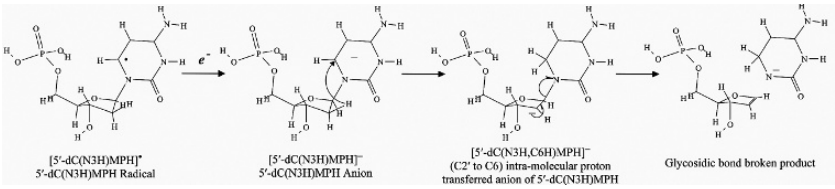

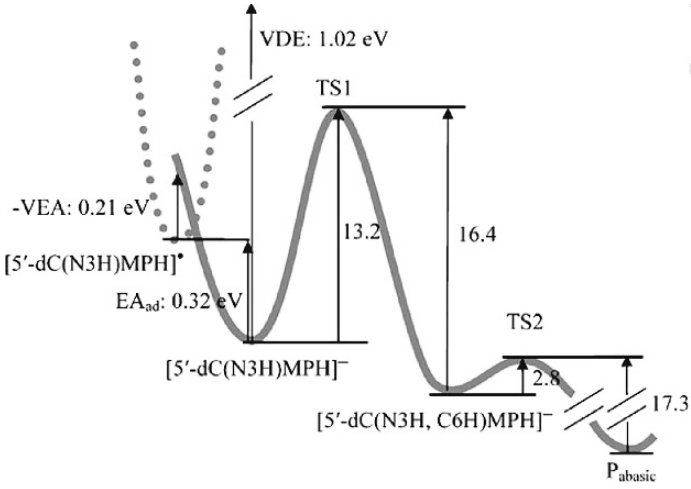

Figure 21-30. The potential energy surface along the pathway leading to the formation of the abasic site (Pabasic). The energy is in kcal/mol^{-1}, except when otherwise indicated (Scheme 2 and Figure 2 of ref. [78]. Reprinted with permission.)

break formation from the anion of hydrogenated nucleotide is ca. 7.6×10^{10} sec^{-1}, which makes the proposed mechanism very probable. At first glance this mechanism may rise concerns since it requires that either H• and a low-energy electron or two low-energy electrons interact with the same nucleotide. This scenario is, however, plausible because high-energy particles create in aqueous systems the so-called "spurs", which contain high concentrations of reactive species, such as radicals and low-energy electrons [1, 2]. Hence, these nucleotides which are in the neighborhood of a "spur" region can be exposed to many reactive species, including H radicals and low-energy electrons.

An analogous mechanism has been employed recently by Gu et al. [78] to suggest that LEEs might induce the formation of an abasic site at the 3′ end of a DNA double helix with a strand ended with a cytidine residue. A large thermodynamic stimulus for the overall process and a low kinetic barrier of the rate-controlling step (Figure 21-30) indicate that LEE attachment to the DNA helix might significantly contribute to this type of DNA damage.

21.4. CONCLUDING REMARKS

Since Sanche's discovery that low-energy electrons are able to trigger single and double strand breaks in DNA, the mechanism of the process has been extensively studied by several experimental and theoretical groups. A number of experimental observations indicate that electron transfer from a nucleobase to the phosphate group might be the main route of SSB formation. The resonance character of the damage yield function suggests that electron transfer might proceed directly from a resonance anion – a hypothesis that was promoted in a series of papers from the Simon group [29, 92, 93]. In this model the rate of SSB formation has to compete with short lifetimes of resonance states. Thus very low barriers are required to explain the SSB yield observed experimentally [1, 2].

A mechanism based on the formation of a stable anionic species could be an alternative for the nonadiabatic mechanism proposed by the Simons group [36, 78–80]. Indeed, in a series of studies, described in the previous sections, we showed that in the presence of species having proton-donor properties the stable valence anions of nucleobases rather than resonances are formed. In fact, even relatively weak interactions as those present in the uracil-water complex are sufficient to render the valence uracil anion to be adiabatically stable in the gas phase. In DNA, even when its "dry" form, as employed in Sanche's experiments, the interactions of nucleobases with water as well as with complementary bases are present. Moreover, in cellular environment the spectrum of species capable of interacting with nucleobases extends to water from physiological solution and various proteins such as histones, replication and DNA repair enzymes. Therefore, the formation of adiabatically stable anions (and their further involvement in the SSB-type damage), via direct electron attachment to nucleobases bound in nucleotides or through the BFPT/PT process that follows the electron attachment, is highly probable both in "dry" DNA irradiated with electrons and in cellular DNA during radiolysis.

So far, two different mechanisms of single strand break formation based on adiabatically stable anions have been proposed. The first mechanism, suggested by the Leszczynski group, assumes the formation of stable anions of 3′- and 5′-phosphates of thymidine and cytidine in which the cleavage of the C-O bond take place via the S_N2-type process. The second reaction sequence, proposed by us, starts from the electron induced BFPT process followed by the second electron attachment to the pyrimidine nucleobase radical, intramolecular proton transfer, and the C-O bond dissociation. In both mechanisms the bottleneck step is associated with very low kinetic barrier which enables the SSB formation to be completed in a time period much shorter than that required for the assay of damage.

A large body of experimental and theoretical data concerning the interaction of LEEs with DNA has been gathered so far. It seems, however, that still many questions are waiting to be resolved. In our future studies we plan to: (i) extend our investigations to systems in which single nucleotides interact with complementary base or nucleotide; (ii) employ hybrid methods MM/QM or QM/QM which will enable the reaction in small fragments of double-stranded DNA to be described. This approach will allow studying the influence of DNA structure on the reactivity

of primary anionic species; (iii) investigate the impact of interactions between nucleotides and fragments of proteins on the cleavage of DNA strand; (iv) study the relationship between nucleobases sequence and proton transfer induced by an excess electron as well as coupling of this process to electron transfer along the DNA helix.

Last but not least, one should realize that this intriguing and very interesting problem of DNA damage possesses at least two practical aspects. First, humans might be endangered by the toxic effects of high-energy radiation, i.e. low-energy electrons, due to exposure to high doses of ionizing radiation during ecological catastrophes or exposures to medium or small doses of high-energy radiation in the course of professional exposure, radiotherapy or medical examinations. Hence, comprehension of the mechanism of DNA damage induced by low-energy electrons could enable the invention of effective means for human protection against the impact of ionizing radiation. Second, DNA would be an ideal, cheap and self-organizing nanowire if it were to be resistant to the presence of excess electrons. Therefore, elucidation of the mechanism of DNA strand-breaks developing during the interactions of polymers with low-energy electrons should enable chemically-modified biomolecules, which would be insensitive to excessive electrons, to be synthesized.

ACKNOWLEDGEMENTS

J.R. gratefully acknowledges stimulating discussions with Prof. Nigel Mason. We would also like to thank the referee for his/her valuable comments concerning the link between transient and stable anions. This work was supported by: (i) Polish State Committee for Scientific Research (KBN) Grants: DS/8221-4-0140-7 (J.R.), KBN/1T09A04930 (K.M.), KBN/N204 077 32/2179 (M.K.) and KBN/N204 127 31/2963 (M.H.), (ii) European Social Funds (EFS) ZPORR/2.22/II/2.6/ARP/U/2/05 (M.H.), (iii) US DOE Office of Biological and Environmental Research, Low Dose Radiation Research Program (M.G.). This material is also based upon work supported by the (U.S.) National Science Foundation under Grant No. CHE-0517337 (K.H.B.). M.H. holds the Foundation for Polish Science (FNP) award for young scientists. I.D. acknowledges the Marie Curie Fellowship.

REFERENCES

1. Sanche L (2002). Nanoscopic aspects of radiobiological damage: fragmentation induced by secondary low-energy electrons. Mass Spectrom Rev 21: 349–369.
2. Sanche L (2005). Low energy electron-driven damage in biomolecules. Eur Phys J D 35: 367–390.
3. Nikjoo H, Charlton DE, Goodhead DT (1994). Monte Carlo track structure studies of energy deposition and calculation of initial DSB and RBE. Ad Space Res 14: 161–180.
4. Prise KM, Folkard M, Michael BD, Vojnovic B, Brocklehurst B, Hopkirk A, Munro IH (2000). Critical energies for SSB and DSB induction in plasmid DNA by low-energy photons: Action spectra for strand-break induction in plasmid DNA irradiated in vacuum. Int J Radiat Biol 76: 881–890.
5. von Sonntag C (1987). The chemical basis for radiation biology. London: Taylor and Francis.

6. Zheng Y, Cloutier P, Hunting DJ, Sanche L, Wagner JR (2005). Chemical basis of DNA sugar-phosphate cleavage by low-energy electrons. J Am Chem Soc 127: 16592–16598.
7. Jay A, LaVerne JA, Simon M, Pimblott SA (1995). Electron energy loss distributions in solid and gaseous hydrocarbons. J Phys Chem 99: 10540–10548.
8. Pimblott SM, LaVerne JA (2007). Production of low-energy electrons by ionizing radiation. Rad Phys Chem 76: 1244–1247.
9. Pogozelski WK, Tullius TD (1998). Oxidative strand scission of nucleic acids: Routes initiated by hydrogen abstraction from the sugar moiety. Chem Rev 98: 1089–1107.
10. Burrows CJ, Muller JG (1998). Oxidative nucleobase modifications leading to strand scission. Chem Rev 98: 1109–1152.
11. Folkard MK, Prise M, Vojnovic B, Davies S, Roper MJ, Michael BD (1993). Measurement of DNA damage by electrons with energies between 25 and 4000 eV. Int J Radiat Biol 64: 651–658.
12. Boudaiffa B, Cloutier P, Hunting D, Huels MA, Sanche L (2000). Resonant formation of DNA strand breaks by low-energy (3 to 20 eV) electrons. Science 287: 1658–1660.
13. Boudaiffa B, Hunting DJ, Cloutier P, Huels MA, Sanche L (2000). Induction of single- and double-strand breaks in plasmid DNA by 100–1500 eV electrons. Int J Radiat Biol 76: 1209–1221.
14. Huels MA, Boudaiffa B, Cloutier P, Hunting D, Sanche L (2003). Single, double, and multiple double strand breaks induced in DNA by 3–100 eV electrons. J Am Chem Soc 125: 4467–4477.
15. Zheng Y, Cloutier P, Hunting DJ, Wagner JR, Sanche L (2006). Phosphodiester and N-glycosidic bond cleavage in DNA induced by 4–15 eV electrons. J Chem Phys 124: 064710–064719.
16. Hotop H, Ruf MW, Allan M, Fabrikant II (2003). Resonance and threshold phenomena in low-energy electron collisions with molecules and clusters. At Mol Opt Phys 49: 85.
17. Pan X, Cloutier P, Hunting D, Sanche L (2003). Dissociative electron attachment to DNA. Phys Rev Lett 90: 208102–1–4.
18. Martin F, Burrow PD, Cai Z, Cloutier P, Hunting DJ, Sanche L (2004). DNA strand breaks induced by 0–4 eV electrons: The role of shape resonances. Phys Rev Lett 93: 068101–1–4.
19. Abdoul-Carime H, Cloutier P, Sanche L (2001). Low-energy (5–40 eV) electron-stimulated desorption of anions from physisorbed DNA bases. Radiat Res 155: 625–633.
20. Pan X, Abdoul-Carime H, Cloutier P, Bass AD, Sanche L (2005). D-, O- and OD- desorption induced by low-energy (0–20 eV) electron impact on amorphous D2O films. Radiat Phys Chem 72: 193–199.
21. Antic D, Parenteau L, Lepage M, Sanche L (1999). Low-energy electron damage to condensed-phase deoxyribose analogues investigated by electron stimulated desorption of H^- and electron energy loss spectroscopy. J Phys Chem B 103: 6611–6619.
22. Panajotovic R, Martin F, Cloutier P, Hunting D, Sanche L (2006). Effective cross sections for production of single- strand breaks in plasmid DNA by 0.1 to 4.7 eV electrons. Radiat Res 165: 452–459.
23. Aflatooni K, Gallup GA, Burrow PD (1998). Electron attachment energies of the DNA bases. J Phys Chem A 102: 6205–6207.
24. Allan M (1989). Study of triplet states and short-lived negative ions by means of electron impact spectroscopy. J Electron Spectrosc Relat Phenom 48: 219–351.
25. Grandi A, Gianturco FA, Sanna N (2004). H^- Desorption from uracil via metastable electron capture. Phys Rev Lett 93: 048103–1–4.
26. Zheng Y, Wagner JR, Sanche L (2006). DNA damage induced by low-energy electrons: Electron transfer and diffraction. Phys Rev Lett 96: 208101–1–4.
27. Ptasinska S, Sanche L (2007). Dissociative electron attachment to abasic DNA. Phys Chem Chem Phys 9: 1730–1735.

28. Cai Z, Cloutier P, Hunting D, Sanche L (2005). Comparison between X-ray photon and secondary electron damage to DNA in vacuum. J Phys Chem B 109: 4796–4800.
29. Simons J (2006). How do low-energy (0.1–2 eV) electrons cause DNA-strand breaks? Acc Chem Res 39: 772–779.
30. Voityuk AA (2006). In: Sponer J, Lankas F., (eds.), Leszczynski, J. (ser. ed.), Computational modeling OD charge transfer in DNA in Chalenges and Advances in Computational Chemistry and Physics, vol 2: Computational Studies of RNA and DNA. Springer, The Netherlands, pp. 485–512.
31. Voityuk AA, Siriwong K, Roesch N (2001). Charge transfer in DNA. Sensitivity of electronic couplings to conformational changes. Phys Chem Chem Phys 3: 5421–5425.
32. Sadowska-Aleksiejew A, Rak J, Voityuk AA (2006). Effect of intra base-pairs on hole transfer coupling in DNA. Chem Phys Lett 429: 546–550.
33. Svozil D, Jungwith P, Havlas Z (2004). Electron binding to nucleic acid bases. Experimental and theoretical studies. A review., Collect Czech Chem Commun 69: 1395–1428.
34. Hendricks JH, Lyapustina SA, de Clercq HL, Bowen KH (1998). The dipole bound-to-covalent anion transformation in uracyl. J Chem Phys 108: 8–11.
35. Yan M, David Becker D, Summerfield S, Renke P, Sevilla MD (1996). Relative abundance and reactivity of primary ion radicals in γ-irradiated DNA at low temperatures. 2. Single- vs Double-Stranded DNA. J Phys Chem 96: 1983–1989.
36. Dąbkowska I, Rak J, Gutowski M (2005). DNA strand breaks induced by concerted interaction of H radicals and low-energy electrons: A computational study on the nucleotide of cytosine. Eur Phys J D 35: 429–435.
37. Lu Q-B, Bass AD, Sanche L (2002). Superinelastic electron transfer: Electron trapping in H_2O ice via the N_2^- ($^2\Pi_g$) resonance. Phys Rev Lett 88: 17601–1–4.
38. Li X, Grubisic A, Stokes ST, Cordes J, Ganteför GF, Bowen KH, Kiran B, Willis M, Jena P, Burgert R, Schnöckel H (2007). Unexpected stability of Al_4H_6: A borane analog? Science 315: 356–358.
39. Lindner J, Grotemeyer J, Schlag EW (1990). Applications of multiphoton ionization mass spectrometry: Small protected nucleosides and nucleotides. Int J Mass Spectrom Ion Proc 100: 267–285.
40. Meijer G, de Vries MS, Hunziker HE, Wendt HR (1990). Laser desorption jet-cooling spectroscopy of para-amino benzoic acid monomer, dimer, and clusters. J Chem Phys 92: 7625–7635.
41. Boesl U, Bassmann C, Kaesmeier R (2001). Time of flight mass analyzer for anion mass spectrometry and anion photoelectron spectroscopy. Int J Mass Spect 206: 231–244.
42. Gutowski M, Dąbkowska I, Rak J, Xu S, Nilles JM, Radisic D, Bowen Jr. KH (2002). Barrier-free intermolecular proton transfer in the uracil-glycine complex induced by excess electron attachment. Eur Phys J D 20: 431–439.
43. Haranczyk M, Bachorz R, Rak J, Gutowski M, Radisic D, Stokes ST, Nilles JM, Bowen KH (2003). Excess electron attachment induces barrier-free proton transfer in binary complexes of uracil with H_2Se and H_2S but not with H_2O. J Phys Chem B 107: 7889–7895.
44. Haranczyk M, Rak J, Gutowski M, Radisic D, Stokes ST, Nilles JM, Bowen KH (2004). Effect of hydrogen bonding on barrier-free proton transfer in anionic complexes of uracil with weak acids: $(U\ldots HCN)^-$ versus $(U\ldots H_2S)^-$. Isr J Chem 44: 157–170.
45. Haranczyk M, Dąbkowska I, Rak J, Gutowski M, Nilles JM, Stokes ST, Radisic D, Bowen KH (2004). Excess electron attachment induces barrier-free proton transfer in anionic complexes of thymine and Uracil with Formic Acid. J Phys Chem B 108: 6919–6921.

46. Dąbkowska I, Rak J, Gutowski M, Nilles JM, Radisic D, Bowen Jr KH (2004). Barrier-free intermolecular proton transfer induced by excess electron attachment to the complex of alanine with uracil. J Chem Phys 120: 6064–6071.
47. Dąbkowska I, Rak J, Gutowski M, Radisic D, Stokes ST, Nilles JM, Bowen Jr KH (2004). Barrier-free proton transfer in anionic complex of thymine with glycine. Phys Chem Chem Phys 6: 4351–4357.
48. Haranczyk M, Rak J, Gutowski M, Radisic D, Stokes ST, Bowen KH (2005). Intermolecular proton transfer in anionic complexes of uracil with alcohols. J Phys Chem B 109: 13383–13391.
49. Radisic D, Bowen KH, Dąbkowska I, Storoniak P, Rak J, Gutowski M (2005). AT base pair anions versus (9-methyl-A)(1-methyl-T) base pair anions. J Am Chem Soc 127: 6443–6450.
50. Mazurkiewicz K, Haranczyk M, Gutowski M, Rak J, Radisic D, Eustis SN, Wang D, Bowen KH (2007). Valence anions in complexes of adenine and 9-methyladenine with formic acid: Stabilization by intermolecular proton transfer. J Am Chem Soc 129: 1216–1224.
51. Bachorz RA, Haranczyk M, Dąbkowska I, Rak J, Gutowski M (2005). Anion of the formic acid dimer as a model for intermolecular proton transfer induced by a π^* excess electron. J Chem Phys 122: 204304–1–7.
52. Taylor PR (1994). In: Roos BO (ed.), Lecture notes in quantum chemistry II, Springer, Berlin.
53. Kendall RA, Dunning Jr TH, Harrison RJ (1992). Electron affinities of the first-row atoms revisited. Systematic basis sets and wave functions. J Chem Phys 96: 6796–6806.
54. Allan M (2007). Electron collisions with formic acid monomer and dimer. Phys Rev Lett 98: 123201–1–4.
55. Aflatooni K, Hitt B, Gallup GA, Burrow PD (2001). Temporary anion states of selected amino acids. J Chem Phys 115: 6489–6494.
56. Gutowski M, Skurski P, Simons J (2000). Dipole-bound anions of glycine based on the zwitterion and neutral structures. J Am Chem Soc 122: 10159–10162.
57. Bachorz RA, Rak J, Gutowski M (2005). Stabilization of very rare tautomers of uracil by an excess electron. Phys Chem Chem Phys 7: 2116–2125.
58. Dolgounitcheva O, Zakrzewski VG, Ortiz JV (1999). Anionic and neutral complexes of uracil and water. J Phys Chem A 103: 7912–7917.
59. Hendricks JH, Lyapustina SA, de Clercq HL, Bowen KH (1998). The dipole bound-to-covalent anion transformation in uracil. J Chem Phys 108: 8–11.
60. Dąbkowska I, Gutowski M, Rak J (2002). On the stability of uracil-glycine hydrogen-bonded complexes: A computational study. Pol J Chem 76: 1243–1247.
61. Dąbkowska I, Rak J, Gutowski M (2002). Computational study of hydrogen-bonded complexes between the most stable tautomers of glycine and uracil. J Phys Chem A 106: 7423–7433.
62. Becke AD (1988). Density-functional exchange-energy approximation with correct asymptotic behavior. Phys Rev A 38: 3098–3100.
63. Becke AD (1993). Density-functional thermochemistry. III. The role of exact exchange. J Chem Phys 98: 5648–5652.
64. Lee C, Yang W, Paar RG (1988). Development of the Colle-Salvetti correlation energy formula into a functional of the electron density. Phys Rev B 37: 785–789.
65. Ditchfield R, Hehre WJ, Pople JA (1971). Self-consistent molecular-orbital methods. IX. An extended gaussian-type basis for molecular-orbital studies of organic molecules. J Chem Phys 54: 724–728.
66. Hehre WJ, Ditchfield R, Pople JA (1972). Self-consistent molecular orbital Methods. XII. Further extensions of gaussian-type basis sets for use in molecular orbital studies of organic molecules. J Chem Phys 56: 2257–2261.

67. Mazurkiewicz K, Haranczyk M, Gutowski M, Rak J, Radisic D, Eustis SN, Wang D, Bowen KH (2007). Valence anions in complexes of adenine and 9-methyladenine with formic acid: Stabilization by intermolecular proton transfer. J Am Chem Soc 129: 1216–1224.
68. Haranczyk M, Gutowski M, Li X, Bowen KH (2007). Bound anionic states of adenine. Theoretical and photoelectron spectroscopy study. Proc. Natl Acad Sci USA 104: 4804–4807.
69. Haranczyk M, Gutowski M (2005). Valence and dipole-bound anions of the most stable tautomers of guanine. J Am Chem Soc 127: 699–706.
70. Haranczyk M, Gutowski M (2005). Finding adiabatically bound anions of guanine through a combinatorial computational approach. Angew Chem Int Ed 44: 6585–6587.
71. Periquet V, Moreau A, Carles S, Schermann J, Desfrancois CJ (2000). Cluster size effects upon anion solvation of N-heterocyclic molecules and nucleic acid bases. J Electron Spectrosc Relat Phenom 106: 141–151.
72. Jalbout A, Adamowicz L (2001). Dipole-bound anions of adenine-water clusters. Ab initio study. J Phys Chem A 105: 1033–1038.
73. Jalbout A, Adamowicz L (2002). Cluster size effects upon stability of adenine–methanolanions. Theoretical study. J Mol Struct 605: 93–10.
74. Bally T, Sastry GN (1997). Incorrect dissociation behavior of radical ions in density functional calculations. J Phys Chem A 101: 7923–7925.
75. Storoniak P, Kobyłecka M, Dąbkowska I, Rak J, Gutowski M (2007). Comparison of intermolecular proton transfer in the Watson-Crick anionic guanine-cytosine and 8-oxoguanine-cytosine pairs. To be submitted.
76. Li X, Cai Z, Sevilla MD (2001). Investigation of proton transfer within DNA base pair anion and cation radicals by density functional theory (DFT). J Phys Chem B 105: 10115–10123.
77. Becker D, Sevilla MD (1993). In: Advances in radiation biology, the chemical consequences of radiation damage to DNA. Academic Press, New York.
78. Gu J, Wang J, Rak J, Leszczynski L (2007). Findings on the electron-attachment-induced abasic site in a DNA double helix. Angew Chem Int Ed 46: 3479–3481.
79. Bao X, Wang J, Gu J, Leszczynski J (2006). DNA strand breaks induced by near-zero-electronvolt electron attachment to pyrimidine nucleotides. Proc Nat Acad Sci USA 103: 5658–5663.
80. Gu J, Wang J, Leszczynski L (2006). Electron attachment-induced DNA single strand breaks: $C_{3'}$-$O_{3'}$ sigma-bond breaking of pyrimidine nucleotides predominates. J Am Chem Soc 128: 9322–9323.
81. Wesolowski SS, Leininger ML, Pentchev PN, Schaefer HG III (2001). Electron affinities of the DNA and RNA bases. J Am Chem Soc 123: 4023–4028.
82. Schiedt J, Weinkauf R, Neumark DN, Schlag E (1998). Anion spectroscopy of uracil, thymine and the amino-oxo and amino-hydroxy tautomers of cytosine and their water clusters. Chem Phys 239: 511–524.
83. Kawai K, Saito I (1998). Stabilization of Hoogsteen base pairing by introduction of NH_2 group at the C8 position of adenine. Tetrahedron Lett 29: 5221–5224.
84. Hoffman MM, Kharpov MA, Cox JC, Yao J, Tong J, Ellington AD (2004). AANT: The Amino Acid–Nucleotide Interaction Database. Nucleic Acid Res 32: D174–D181.
85. Mazurkiewicz K, Rak J (2007). Purine nucleobases as possible electron traps in DNA-protein complexes. To be submitted.
86. Mazurkiewicz K (2007). Electron attachment and intra- as well as intermolecular proton transfer in the nucleobases related systems – relevance for DNA damage by low energy electrons. Ph.D. thesis. University of Gdańsk, Gdańsk, Poland.
87. Alan C, Cheng AC, William W, Chen WW, Cynthia N, Fuhrmann CN, Alan D, Frankel AD (2003). Recognition of nucleic acid bases and base-pairs by hydrogen bonding to amino acid side-chains. J Mol Biol 327: 781–796.

88. Mazurkiewicz K, Haranczyk M, Gutowski M, Rak J (2007). Can an excess electron localize on a purine moiety in the adenine-thymine Watson-Crick base pair? A computational study. Int J Quantum Chem DOI: 10.1002/qua.21359.
89. Cheng AC, Chen WW, Fuhrmann CN, Frankel AD (2003). Recognition of nucleic acid bases and base-pairs by hydrogen bonding to amino acid side-chains. J Mol Biol 327: 781–796.
90. Haranczyk M, Mazurkiewicz K, Gutowski M, Rak J, Radisic D, Eustis S, Wang D, Bowen KH (November 3rd–4th 2006). Purine moiety as an excess electron trap in the Watson-Crick AT pair solvated with formic acid. A Computational and Photoelectron Spectroscopy Study, 15th Conference on Current Trends in Computational Chemistry, Jackson, Mississippi, USA.
91. Li X, Sevilla MD, Sanche L (2003). Density functional theory studies of electron interaction with DNA: Can zero eV electrons induce strand breaks? J Am Chem Soc 125: 13668–13669.
92. Berdys J, Skurski P, Simons J (2004). Damage to model DNA fragments by 0.25–1.0 eV electrons attached to a thymine π^* orbital. J Phys Chem B 108: 5800–5805.
93. Berdys J, Anusiewicz I, Skurski P, Simons J (2004). Theoretical study of damage to DNA by 0.2–1.5 eV electrons attached to cytosine. J Phys Chem A 108: 2999–3005.
94. Rienstra-Kiracofe JC, Tschumper GS, Schaefer HF, Nandi S, Ellison GB (2002). Atomic and molecular electron affinities: Photoelectron experiments and theoretical computations. Chem Rev 102: 231–282.
95. Gu J, Xie Y, Schaefer HF (2006). Near 0 eV electrons attach to nucleotides. J Am Chem Soc 128: 1250–1252.
96. Gu J, Xie Y, Schaefer HF (2005). Glycosidic bond cleavage of pyrimidine nucleosides by low energy electrons: A theoretical rationale. J Am Chem Soc 127: 1053–1057.
97. Tomasi J, Perisco M (1994). Molecular interactions in solution: An overview of methods based on continuous distributions of the solvent. Chem Rev 94: 2027–2094.
98. Kumar A, Sevilla MD (2007). Low-energy electron attachment to 5′-Thymidine monophosphate: Modeling single strand breaks through dissociative electron attachment. J Phys Chem B 111: 5464–5474.
99. Colson AO, Sevilla MD (1995). Elucidation of primary radiation damage in DNA through application of ab initio molecular orbital theory. Int J Radiat Biol 67: 627–645.
100. Li X, Cai Z, Sevilla MD (2002). Energetics of the radical ions of the AT and AU base pairs: A density functional theory (DFT) study. J Phys Chem A 106: 9345–9351.
101. Lynch BJ, Fast PL, Harris M, Truhlar DG (2000). Adiabatic connection for kinetics. J Phys Chem A 104: 4811–4815.